Detection, Synchronization, Channel Estimation and Capacity in UWB Sensor Networks using Compressed Sensing

by

Shao-Yuan Chen

A dissertation submitted in partial fulfillment
of the requirements for the degree of
Doctor of Philosophy
(Electrical Engineering: Systems)
in The University of Michigan
2014

Doctoral Committee:

Professor Wayne E. Stark, Chair
Associate Professor Achilleas Anastasopoulos
Associate Professor Anna C. Gilbert
Associate Professor David D. Wentzloff

ACKNOWLEDGEMENTS

TABLE OF CONTENTS

LIST OF FIGURES

Figure

LIST OF TABLES

ABSTRACT

Detection, Synchronization, Channel Estimation and Capacity in UWB Sensor
Networks using Compressed Sensing

by

Shao-Yuan Chen

Chair: Wayne E. Stark

Conventional receivers in ultrawideband (UWB) communication system usually require high sampling rate and thus consume much power. With compressed sensing (CS), the sampling rate can potentially be reduced. In this thesis, the performance of CS used in a UWB receiver is evaluated. Using a compressed sensing approach, the receiver consists of a number of analog correlators that process the received signal by projecting the received signal using random (or pseudo random) vectors. Considering the practical implementation in the receiver, the orthogonal Hadamard vectors in the correlators are adopted. After projection, the matching pursuit or basis pursuit is used to obtain the channel estimate. The recovered channel templates are then correlated with received signal to detect the transmitted information bits.

The bit error rate (BER) performance of systems with different number of pilots, projection vectors, and fingers in a rake receiver is also evaluated. Moreover, the performance of different receivers and the effect of the finite bit resolution on channel estimation is investigated. It is shown that the sampling rate can be reduced significantly with only a slight degradation in performance when a compressed projection

matrix is used compared to when a conventional Nyquist sampling rate is applied.

A second aspect of UWB investigated is channel measurement and corresponding channel capacity. The measurement data of a channel between the UWB antennas under the bridge across Telegraph Road in Michigan is used to calculate the channel capacity. The channel capacity calculated in this specific environment provides the knowledge of the fundamental limit of rate of transmission in this particular scenario.

A third aspect of UWB communication considered involves the synchronization and detection of signal presence. An m-sequence is used to synchronize the signal. The corresponding BER performance is evaluated. It is observed that the BER performance of the proposed synchronization method is comparable to that of a system assumed to have perfect synchronization. Finally, the autocorrelation characteristic of the signal is exploited to detect the existence of the signal. The advantage of the method proposed is that the threshold to determine the existence of signals is independent of signal-to-noise ratio.

CHAPTER I

Introduction

1.1 Motivation

Ultra-wideband (UWB) communication has drawn considerable attention recently for various applications including high data rate, short distance and low data rate, long distance communication scenarios. It is suitable for a system that requires high-bandwidth, low power, and shared spectrum such as sensor data collection, high precision location, and navigation [20]. One traditional form of UWB communication is known as impulse radio (IR), in which ultra-short pulses that are nanoseconds in duration are used to transmit data. The benefits of transmitting data using ultra-short pulses are as follows. First, a simple transmitter can be used because no upconversion is used. Second, the transmitted signal power is distributed over an ultra-wide bandwidth with small power density, which creates little interference to other communication systems within the same bandwidth. Third, it is possible to increase the resolution of delay and thus generate a rich multipath structure, allowing diversity.

As mentioned above, although UWB transmitters are simple, receivers encounter the following challenges: timing synchronization and channel estimation. Channel estimation is a critical issue in UWB because the transmitted signal is split into many small amplitude multipath components by the channel. The multipath components need to be properly combined by UWB receivers so that sufficient energy is collected

for each bit to be accurately detected by the receivers. One challenge in this process is to estimate the strength of a path, which is especially difficult for small amplitude paths. Several papers in the field proposed several solution to address the problem of channel estimation. According to [19], to obtain accurate UWB channel estimation, it may be necessary to have 25 samples for one pulse (also called monocycle) with a duration on the order of a nanosecond, that is up to 25 GHz. To operate at this speed, a interleaved flash ADC [2] or a set of polyphase ADCs [26] may be needed. However, the former often has low bit resolution, high power consumption and cost, and large circuit area; the latter is built with high circuit complexity resulting from precise timing control. To address these issues, there is a need for UWB receiver designs that can reduce the sampling rate. One such design is the transmitted reference (TR) approach in [15], which reduces the sampling rate, but results in poor channel estimation at low signal-to-noise ratios (SNR). The BER performance with TR method in [15] is shown to be $P_b = Q\left(\left(T_b W + \frac{E_r}{2N_0}\right)^{-1/2} \frac{E_r}{4N_0}\right)$, where W is one-sided bandwidth, T_b is bit duration, E_r is the total received energy, and the noise power is $2N_0 W$. Another is the minimum mean-squre-error (MMSE) rake receiver in [17], which also reduces the sampling rate at each output of the matched filter to one sample per frame instead of one sample per pulse to collect channel parameters. This approach has the drawback of requiring a large amount of processing after the ADC. Unlike the previous approaches, receiver structures using a noisy template (NT) proposed in [31] are more robust on handling mistiming than the rake receiver. However, they suffer from the bit error rate (BER) performance degradation at low SNR.

In this thesis, I address the following problems: 1) Channel estimation using CS, 2) Channel measurement and channel capacity, and 3) Synchronization and detection of UWB signals in multipath fading channels.

1.2   Channel Estimation

To solve the problem of extremely high sampling rate necessary for channel estimation, compressed sensing (CS) [11] has been proposed. In [27], CS and with a simple repetition code with a noisy template and rake receivers was considered. The results in [27] indicated that the performance was better than the performance of a system using binary phase shift keying (BPSK) on an additive white Gaussian noise (AWGN) channel. These results could not be duplicated because the BER performance of an ideal system using BPSK is a lower bound. In this thesis, the result that is consistent with the ideal system using BPSK is presented. Different parameters for receiver designs is also illustrated and compared.

1.3   Channel Measurement and Channel Capacity

In order to investigate the channel capacity, it is necessary to have the channel characteristic. In IEEE 802.15.4a standard [24], several channel models for different scenarios are provided. However, no specific channel model for the environment at the girders under the bridge where the sensors in our project are deployed. Hence, the measurement data of the channel between the antennas of the sensors was collected in a UWB system which are deployed on the bridge crossing over Telegraph road, Michigan. Using these measured data, the channel capacity in this scenario is calculated.

The measurement data is first processed using the CLEAN algorithm to estimate the channel impulse response [16]. With the estimated channel impulse, the result in [14] is applied to calculate the channel capacity corresponding to the measured channel impulse response. The minimum E_b/N_0 required for different scenarios is also evaluated by the theorem in [30]. The value of the required minimum E_b/N_0 depends on whether the transmitter has the knowledge of channel information or not.

1.4 Signal Detection and Synchronization

The performance of channel estimation described above assumed perfect synchronization. To be practical, the assumption of perfect synchronization needs to be relaxed. Moreover, even before the synchronization is accomplished, it is necessary to determine whether the signal of interest is present or not. After detecting the presence of the signals, then signal synchronization can be initiated. To detect the signal presence, Duarte et. al [13] use matching pursuit to extract the largest component in the received signal and compared with some threshold to determine if the signal is present. However, they can only propose that the threshold is chosen to minimize detection error based on Monte Carlo simulation. This algorithm seems to require a long time and is inefficient to implement. Liu et. al [18] addressed this issue and use location information between signal of interest and the signal obtained by prior information. The threshold in their method is dependent of SNR, which is often hard to acquire in advance.

After determining the existence of the signal, the synchronization is needed. Carbonelli et.al [8] [7] applied a least square (LS) method to solve the synchronization and channel estimation problem in a UWB system. However, this required a high sampling rate as high as the frequency of the inverse of a pulse duration. Rabbachin and Oppermann [28] exploited an energy collection receiver to achieve low-complexity but the method is not able to acquire the channel estimation at the same time.

1.5 Contribution of Thesis

In this thesis, the performance of a receiver using CS is analyzed. In addition, the analysis is extended to include various receiver architectures as well as error control coding techniques. The BER performance with different numbers of pilot bits, different numbers of projections and different numbers of fingers in a rake receiver is

evaluated. The impact of finite bit resolution used in the system is also studied. The perfomance analysis shows that the sampling rate can be reduced by a factor about 100 with a loss in the BER performance of about 2dB.

The channel capacity based on channel measurements with and without channel knowledge at transmitters is determined. The minimum E_b/N_0 and the corresponding channel capacity are determined with channel measurement data collected at different locations under the I-275 bridge across the Telegraph Road in Michigan. When capacity is larger than 1 bit per channel use, one can observe a 5 dB gap between the case that the transmitter has channel information and the case that the transmitter has no channel information. On the other hand, the gap increases at low rates.

The algorithms for detection of signal presence and signal synchronization using compressed sensing is developed. The proposed method utilizes the autocorrelation of repeated signals to detect existence of signals in such a way that the threshold can be predetermined and is independent of SNR. Using maximum length sequences, the frame offsets of received signals can be determined and then compensated. The BER performance of receivers adopting the proposed synchronization algorithm is shown to be close to the receivers with perfection synchronization. In addition, the sampling rate with CS is reduced to be the same as the frame rate because of compressed sensing and the channel estimation is performed at the same time.

1.6 Outline of Thesis

The rest of this thesis is organized as follows. in Chapter II, a review of CS and matching pursuit (MP) is introduced. The system model and different receiver structures, coding schemes are descirbed. Simulation results with respect to different parameters and receiver structures and the effect of quantization are shown in Chapter III. The channel capacity calculated from the channel measurement data collected under the bridge is investigated in Chapter IV. The algorithm to detect the existence

of signals and the signal synchronization is described in Chapter V . Conclusions and suggestions for future research are discussed in Chapter VI.

CHAPTER II

Background of Compressed Sensing

2.1 Compressed Sensing

The compressed sensing (CS) theorem shows that one can sample the signal of interest with much fewer samples than that with Nyquist rate and recover it with high probability as long as some criteria is satisfied. The main two criteria are that signal is "sparse" and the vectors in sensing basis is "incoherence" with the vectors in the presentation basis. To realize this theory, one need to know these two important principles of CS: sparsity and incoherence. They are introduced in the following subsections.

2.1.1 Sparsity

Sparsity quantifies the notion that "information" of a continuous-time signal can be much less than that implied by its bandwidth-time product or in the discrete-time signal case, the number of major components of the signal is significantly smaller than its length. In other words, CS use the fact that many signals of interest are sparse and can be further compressed by some appropriate basis. Many signals of interest have sparse representation when decomposed in a proper basis. Consider a signal vector $f \in \Re^n$ in discrete time domain which can be expanded in an orthonormal

basis $\Psi = [\psi_1 \ \psi_2 \ \cdots \psi_n]$ as follows:

$$f = \sum_{i=1}^{n} x_i \psi_i \qquad (2.1)$$

where x_i is the coefficient sequence of f and $x_i = \langle f, \psi_i \rangle$. One can write $f = \Psi x$, where Ψ is the $n \times n$ matrix with the column vectors $\psi_1, \psi_2, \ldots, \psi_n$. If one can drop the negligible coefficients without noticeable loss, it is defined that the signal is sparse. Define $f_S := \Psi x_S$, where x_S represent the vector of coefficients (x_i) with the smalles $n - S$ components set to zero. This vector is called S-sparse because it has S nonzero entries. Since Ψ is an orthonormal basis, $\|f - f_S\|_2 = \|x - x_S\|_2$, and if the sorted amplitude of x_i's decay substantially, then x_S approximates x well and thus, the error $\|f - f_S\|_2$ is small.

2.1.2   Incoherence

Consider a pair (Φ, Ψ) of orthonormal basis of $\Re^n$. The first basis Φ, called sensing basis, is used to correlate with the signal of interest f: $y_k = \langle f, \phi_k \rangle$, $k = 0, \ldots, m-1$. The second basis Ψ is called the presentation basis.

Definition II.1. The coherence between the sensing basis Φ and the representation basis Ψ is

$$\mu(\Phi, \Psi) = \sqrt{n} \max_{0 \le k, j \le n-1} |\langle \phi_k, \psi_j \rangle| \qquad (2.2)$$

By this definition in [6], the coherence is the largest correlation between any two vectors in the bases Ψ and Φ.

The value of coherence $\mu(\Phi, \Psi)$ can range from 1 to $\sqrt{n}$ [12]. To apply compressed sensing efficiently, low coherence pairs of the two bases Φ and Ψ are essential because low coherence guarentee the possibility of ideal atomic decomposition.[12]

In [6], it is also stated that the random matrices with identically independent distributed (i.i.d.) entries such as Gaussian or ± 1 binary elements also possess a very

low coherence with any basis Ψ. These two kinds of matrices is used in the simulation discussed later.

2.1.3   Undersampling and Sparse Signal Recovery

In the ideal case, it is desired to measure all the n elements of f, but it may be the case that only a set of M measurements is accessible:

$$y_k = \langle f, \phi_k \rangle, \quad k \in M, \tag{2.3}$$

where $M \subset \{1, \dots, n\}$ is a subset of cardinality $m < n$. Using ℓ_1-norm[1] minimization to recover the signal can be accomplished with these measurements from y_k, $k \in M$. The reconstruction $\tilde{f}$ is given by $\tilde{f} = \Psi \tilde{x}$, where $\tilde{x}$ is the solution to the convex optimization problem:

$$\min_{\hat{x} \in \Re^n} \|\hat{x}\|_1 \quad \text{subject to} \quad y_k = \langle \phi_k, \Psi \hat{x} \rangle, \quad \forall k \in M \tag{2.4}$$

In other words, among all the possible signals consistent with the measurement data satisfying $\hat{f} = \Psi \hat{x}$, $\tilde{f}$ is chosen to reconstruct such that the coefficient x_i's has minimal ℓ_1 norm. The ℓ_1 norm minimization can be achieved by basis pursuit (BP) [9] but it is not the only method to recover the signal and some other approaches such as a well-known suboptimal greedy algorithm called matching pursuit (MP) can be used. The MP algorithm will be discussed in Section 2.2.

The following theorem shows that when f is sufficiently sparse, the recovered signal by ℓ_1 normalization is perfectly reconstructed.

Theorem II.2. *[3] Fix $f \in \Re^n$ and suppose that the coefficient sequence x of f in the basis Ψ is S-sparse. Select m measurements in the measurement domain Φ uniformly*

---

[1] ℓ_1-norm: $\|\hat{x}\|_1 = \sum_{i=0}^{n-1} |x_i|$.

at random. Then if

$$m \geq C\mu^2(\Phi, \Psi)S\log(n) \tag{2.5}$$

for some positive constant C, the solution $\tilde{x}$ to (2.4) can be recovered with overwhelming probability.

I would like to point out the following comments. First, the importance of low coherence is obvious. With smaller coherence, the fewer samples are needed. This result explain why compressed sensing is efficient with low coherence discussed previously. First, measuring only a set of m coefficients with m much less than the length of signal n does not result in recovery loss. In particular, if $\mu(\Phi, \Psi)$ is equal or close to one, then it suffices to recover the signal with on the order of $S\log n$ samples instead n. Second, the signal of interest f can be exactly recovered from m measurements by solving the convex optimization problem in (2.4) without knowledge about the number of nonzero entries in x, the position of these nonzero entries, or their amplitudes in advance.

2.1.4   Robustness of Compressed Sensing

In practice, since the signal of interest may not be exactly S-sparse and is often corrupted by noise, CS needs to handle these kinds of scenario to be considered helpful and powerful. Consider the problem of recovering a vector $x \in \Re^n$ from measurements

$$y = Ax + u \tag{2.6}$$

where A is an $m \times n$ "sensing matrix" or "measurement matrix" providing information about x and u is a stochastic or deterministic error term. The formulation in the previous subsection is in the same form if the term u is omitted. Combining the equation $f = \Psi x$ and $y = R\Phi f$, where R is the $m \times n$ matrix collecting the sample components in the subset M. It can be written as $y = R\Phi\Psi x = Ax$ so $A = R\Phi\Psi$.

One need to remember that x in (2.6) can be the coefficient of the signal in a proper basis.

To study the robustness, it is needed to introduce the well-known notion *restricted isometry property* (RIP):

Definition II.3. [5] For each integer $S = 1, 2, \ldots$, define the isometry constant δ_S of a matrix A as the smallest number such that

$$(1 - \delta_S)\|x\|_2^2 \leq \|Ax\|_2^2 \leq (1 + \delta_S)\|x\|_2^2 \tag{2.7}$$

holds for all S-sparse vectors x.

If δ_S is small, the matrix A has the RIP property. It also implies that the matrix A preserves the Euclidean length of S-sparse signals and thus the vector x cannot be in the null space of A. An interpretation of RIP is that all the subsets of S columns extracted by A $(A = R\Phi\Psi)$ are nearly orthogonal to one another. In fact, the columns of A cannot be exactly orthogonal because the number of columns is more than the number of rows. To observe the relation between CS and RIP, assume a S-sparse signal x is obtained with compressed measurement data $y = Ax$. Suppose that δ_{2S} is much less than one so that all pairwise distances between S-spare signals are preserved in the measurement space. In other words, the equation $(1 - \delta_{2S})\|x_1 - x_2\|_2^2 \leq \|Ax_1 - Ax_2\|_2^2 \leq (1 + \delta_{2s})\|x_1 - x_2\|_2^2$ is satisfied and holds for all S-sparse vectors x_1, x_2. The following result guarantees that by the compressed measurement data y, there exists an efficient and robust algorithm for determining S-sparse signals x.

If the RIP is satisfied, then an exact reconstruction of x is given by the following linear program:

$$\min_{\hat{x} \in \Re^n} \|\hat{x}\|_1 \quad \text{subject to} \quad A\hat{x} = y \tag{2.8}$$

Theorem II.4. *[4] Assume that $\delta_{2S} < \sqrt{2} - 1$. The the solution $\tilde{x}$ to (2.8) satisfies*

$$\|\hat{x} - x\|_2 \leq C_0\|x - x_S\|_1/\sqrt{S} \quad and$$

$$\|\hat{x} - x\|_1 \leq C_0\|x - x_S\|_1 \tag{2.9}$$

for some constant C_0, where x_S is the vector x with all but the largest S components set to 0.

Now, consider noisy data and use ℓ_1 norm minimization with weaker constraints for reconstruction:

$$\min_{\hat{x} \in \Re^n} \|\hat{x}\|_1 \quad \text{subject to} \quad \|A\hat{x} - y\|_2 \leq \epsilon, \tag{2.10}$$

where ϵ bounds the amount of noise in the data.

Theorem II.5. *[4] Assume that $\delta_{2S} < \sqrt{2} - 1$. Then the solution $\tilde{x}$ to (2.10) satisfies*

$$\|\hat{x} - x\|_2 \leq C_0\|x - x_S\|_1/\sqrt{S} + C_1\epsilon \tag{2.11}$$

for some constant C_0 and C_1.

According the theorem II.5, the reconstruction error is bounded by the sum of two terms. The first term comes from the error which is possible to occur when the data is noiseless. The second term is proportion to the noise level ϵ. Theorem II.5 also shows that CS is robust to deal with signal that are not sparse and noisy data. To have RIP, one wants to have a sensing matrix with the property that column vectors taken from arbitrary subsets are nearly orthogonal. To obtain such matrices, consider the following random sensing matrices: 1) construct A by sampling n column vectors uniformly at random on a unit sphere of $\Re^m$; 2) construct A by sampling i.i.d. entries from the normal distribution with mean 0 and variance $1/m$;

3) construct A by sampling a random projection P and normalize $A = \sqrt{n/m}$;

4) construct A by sampling i.i.d. entries from a symmetric Bernoulli distribution $P(A_{i,j} = \pm 1/\sqrt{m}) = 1/2$ or other sub-gaussian distribution. One can prove that these matrices satisfies the RIP with very high probability given that

$$m \geq CS\log(n/S) \tag{2.12}$$

where C is some constant depending on each case [1][23]. When (2.12) holds, the probability that randomly constructed matrices do NOT satisfy RIP decays exponentially with m. On the contrary, if (2.12) is not satisfied, no measurement matrix of any kind and no algorithm could produce the result of Theorem II.4. If Ψ is fixed and Φ is constructed as in the previous four listed methods, the matrix $A = \Phi\Psi$ satisfies the RIP with probability approaching one provided that (2.12) holds, where C is some constant depend on each case. These random measurement matrices Φ formed as in 1)-4) are universal. The presentation basis Ψ, which is sparse is not needed to be know when designing the measurement matrix.

2.2   Matching Pursuit

In the previous section, it is indicated that ℓ_1 norm minimization (or so-called basis pursuit (BP)[9]) is just one of ways to recover the signals. BP, however, has high complexity and is not suitable for real-time application. There exist faster and more efficient algorithms exploiting the iterative greedy algorithm with more measurements required to recover the signal, called matching pursuit (MP)[21].

Matching pusuit is a iterative greedy algorithm with simple computation and manages to recover the signal as follows. Matching pursuit first correlates the signal of interest with elements of a basis and chooses the maximal components among them, then removes those components from the signal, and searches again for the vector that

has the strongest correlation with the residual signal. This repetitive procedure stops when only an insignificant signal remains. The signal then can be reconstructed by linear combination of all the vectors selected during the process.

The detailed processes of MP are ordered as follows. First, define the holographic basis $\mathbf{V} = \Phi\Psi = [v_1, v_2, \ldots, v_{N_D}]$, where N_D is the number of vectors in the basis $\mathbf{V}$:

1. Initialization:

   - Set the residual error $e_0 = y$

   - The approximated coefficients $\hat{\Theta} = 0, \hat{\Theta} \in \Re^{N_D}$

   - Set iteration counter $t = 1$

2. Select the vector in the holographic basis that matches the residual error best in the following sense:

$$\ell_t = \arg \max_{i=1,2,\ldots,N_D} \frac{|\langle e_{t-1}, v_i \rangle|}{\|v_i\|} \tag{2.13}$$

3. Update the residual error and the estimate of the coefficient for the selected vector:

$$e_t = e_{t-1} - \frac{\langle e_{t-1}, v_{\ell_t} \rangle}{\|v_{\ell_t}\|^2} v_{\ell_t} \tag{2.14}$$

$$\hat{\theta}_{\ell_t} = \hat{\theta}_{\ell_t} + \frac{\langle e_{t-1}, v_{\ell_t} \rangle}{\|v_{\ell_t}\|^2} \tag{2.15}$$

4. Check for convergence.

   If $t < T_0$ and $\|e_t\|_2 > \epsilon_0 \|y\|_2$, where ϵ_0 is the target residual error, then set $t = t + 1$ and go to step 2; otherwise, go to step 5.

5. Reconstruct the signal estimate as: $\hat{f} = \Psi\hat{\Theta}$.

2.3   Variations of Matching Pursuit

There are some variations of matching pursuit. These variations result from chang-
ing the property of the basis, different number of largest components collected, and
termination criteria. One variation is called orthogonal matching pursuit (OMP) [29].
The main difference between MP and OMP is the method to update the signal resid-
ual. In initialization, the additional index set $\Lambda_0 = \emptyset$ in OMP. Other initialization
is the same as MP. After finding the index ℓ_t such that the vector v_{ℓ_t} maximize the
inner product $|\langle e_{t-1}, v_i \rangle|$, that is, $\ell_t = \arg\max_{i=1,2,\ldots,N_D} |\langle e_{t-1}, v_i \rangle|$ similar to (2.13)
in the second step of MP. The third step for OMP is to update the set Λ_t and the
following steps are shown below [29]:

3. Set $\Lambda_t = \Lambda_{t-1} \cup \{\ell_t\}$.

4. Form the orthogonal projector $\mathbf{P}_t$ on to span$\{v_\ell : \ell \in \Lambda_t\}$.

5. Calculate the new approximation and residual:

$$
\begin{aligned}
a_t &= \mathbf{P}_t \, y \\
e_t &= y - a_t
\end{aligned}
$$

6. Set $t = t + 1$, and return to step 2 if $t < S$, the sparsity level of the signal.

7. The signal estimate $\hat{f}$ has nonzero components at the indices listed in Λ_S. The
   values of the estimate in these components appear in the linear combination:

$$
a_S = \sum_{\ell \in \Lambda_S} \hat{f}_\ell v_\ell \tag{2.16}
$$

The OMP is possible to converge faster than the MP since OMP does not revisit the
same index to update residual signal due to the orthogonal projection. However, the

rich multipath channel diversity in UWB may be lost in the orthogonal property in the OMP. Another variation is named compressive sampling matching pursuit (CoSaMP) [25], which is based on the OMP. Consider an S-sparse signal x, a sampling matrix Φ, and compressed samples $y = \Phi x$. Define the restriction Φ_Λ of the sampling matrix Φ as the column submatrix whose columns are listed in the set Λ. Moreover, define the pseudoinverse of the matrix Φ_Λ, by $\Phi_\Lambda^\dagger = (\Phi_\Lambda^* \Phi_\Lambda)^{-1} \Phi_\Lambda^*$. Denote x_r for the signal that is formed by restricting x to its r largest components. In addition, define $\mathrm{supp}(x) = \{j : x_j \neq 0\}$ and define the restriction of the signal to the set Λ as

$$
x_{|\Lambda} = \begin{cases} x_i, & i \in \Lambda \\ 0, & \text{otherwise.} \end{cases} \tag{2.17}
$$

The CoSaMP can be described as follows

1. Initialization:

   - Set the approximated signal $a^0 = 0$

   - Set the residual signal $e = y$

   - Set the counter $t = 0$

2. Set $t = t + 1$

3.
   - Form signal proxy $\hat{x} = \Phi^* e$

   - Identify large components: $\Upsilon = \mathrm{supp}(\hat{x}_{2S})$

   - Merge supports: $\Lambda = \Upsilon \cup \mathrm{supp}(a^{t-1})$

4.
   - Signal estimation by least-squares: $c_{|\Lambda} = \Phi_\Lambda^\dagger y$

   - Prune to obtain next approximation: $c_{|\Lambda^c} = 0$

5. Update residual samples:

16

- $a^t = c_s$

- $e = y - \Phi a^t$

6. Check termination criterion

In the CoSaMP, some operation is dependent on the sparsity S but it is hard to know know the exact sparsity of the channel impulse response since the number of delay paths is random. Hence, the MP is used in the simulation shown in Chapter III.

CHAPTER III

Channel Estimation and System Analysis

3.1 System Model

3.1.1 UWB Transmitted Signal and Coding Scheme

Consider a simple communication system that uses ultra-short pulses $p(t)$. When sending N_f pulses $p(t)$, the kth binary information bit is transmitted with bit duration T_b. Define $b(k) \in \{-1, 1\}$ as the binary information bit that is transmitted in the interval $[kT_b, (k+1)T_b]$ and modulates the amplitude of the pulses, and $p(t)$ is the pulse with duration $T_p \ll T_f$. The frame duration $T_f = T_b/N_f$ is the time interval between the starting time of two consecutive pulses. Therefore, N_f nonoverlapped pulses are transmitted for each T_b. The transmitted signal can be written as

$$s(t) = \sum_k b(k) \sum_{j=0}^{N_f-1} p(t - jT_f - kT_b) \tag{3.1}$$

Figure 3.1 shows the signal described above.

The N_f identical pulses are a repetition code. Consider an orthogonal code using a Hadamard matrix coding scheme as an alternative. Hadamard matrices are matrices of 1's and -1's whose columns are orthogonal and the conventional size is a power of

18
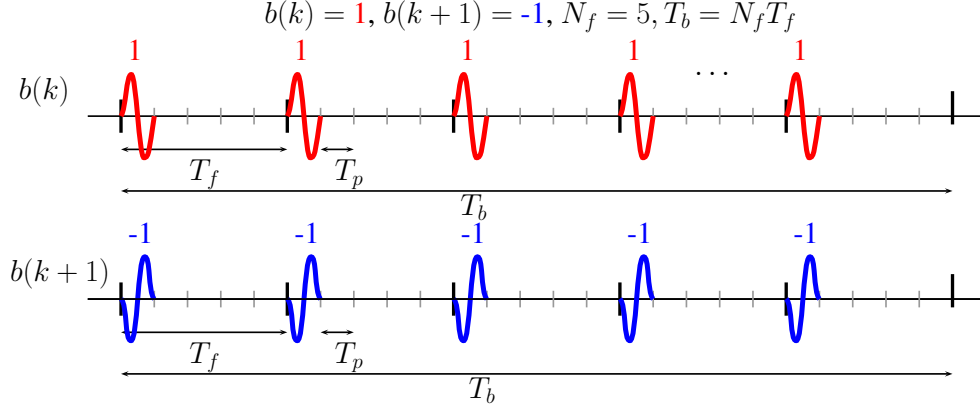
Figure 3.1: Transmitted signals

2. For example, the size 4 Hadamard matrix is as follows:

$$H_4 = \begin{bmatrix} 1 & 1 & 1 & 1 \\ 1 & -1 & 1 & -1 \\ 1 & 1 & -1 & -1 \\ 1 & -1 & -1 & 1 \end{bmatrix}.$$

The advantages of using Hadamard matrix are easy implementation and coding gain relative to the repetition code.

In a Hadamard matrix coding scheme, information bits are divided into blocks of m bits and a sequence of m bits is mapped into 2^m frames of pulses. Since there are 2^m possible different code words for each block, generate a 2^m-by-2^m Hadamard matrix and use different row vectors to represent different code words. For example, if $m = 2$, the two information bits are mapped into 4 frames of transmitting pulses.

Denote the block duration as $T_B = 2^m T_f$, representing m bits with 2^m frames, $H_{2^m}^{\underline{b}(k)}(j)$ is the notation for the jth element in the $\underline{b}(k)$-th row of the Hadamard matrix and $\underline{b}(k)$ is the kth block of m transmitted bits. The transmitted signals using

a Hadamard code can then be written as:

$$s_H(t) = \sum_k \sum_{j=0}^{N_f-1} H_{2^m}^{\underline{b}(k)}(j)p(t - jT_f - kT_B) \tag{3.2}$$

For example, for $m = 2$, if $\underline{b}(k) = [00]$ (in binary), then the first row of the Hadamard matrix is selected, that is, $H_4^{\underline{b}(k)} = [+1, +1, +1, +1]$ and $H_4^{\underline{b}(k)}(j) = 1$ for $j = 1, 2, 3, 4$.

3.1.2 Channel Model

The multipath channel considered can be described by the following impulse response:

$$h(t) = \sum_{\ell=0}^{L-1} \alpha_\ell \delta(t - \tau_\ell) \tag{3.3}$$

where $\delta(\cdot)$ is the dirac delta function, τ_ℓ and α_ℓ are the delay and the gain associated with the ℓ-th propagation path of the UWB channel and L is the number of propagation paths. The channel $h(t)$ is assumed to be static during the transmission of N_s consecutive bits and assume $T_f \geq \tau_{L-1} + T_p$, where τ_{L-1} is the maximum delay spread of the multipath channel $h(t)$, so no interpulse interference occurs.

Henceforth, the repetition code scheme is considered to derive the equations for received signals. In this scenario, the received signal of the first frame of the kth transmitted information bit without noise can be written as

$$r_{f,k}(t) = b(k) \cdot \sum_{\ell=0}^{L-1} \alpha_\ell p(t - kT_b - \tau_\ell). \tag{3.4}$$

Here, $r_{f,k}(t)$ is the sum of scaled and delayed versions of the transmitted pulse $p(t)$. Under the assumption that $T_f \geq \tau_{L-1} + T_p$, the received signal for the kth bit can be expressed by periodically repeating the term $r_{f,k}(t)$ every T_f seconds. The received

signal corresponding to the k-th transmitted bit is then

$$r_k(t) = \sum_{j=0}^{N_f-1} r_{f,k}(t - jT_f) + w(t) \qquad (3.5)$$

where $w(t)$ is a zero-mean additive white Gaussian noise (AWGN) process which represents the thermal noise and multiuser interference. Two receiver designs can take advantage of multipath diversity of the UWB channel. One is the rake receiver [19] and the other is the correlator based detector [20], both of which require estimation of the channel and assume that the receivers has an estimate of the path delays and path gains of the UWB channel. The process of these two kinds of receivers will be discussed in detail later. One common estimation involves a data-aided framework. I use N_p known pilot bits to estimate the channel impulse response in each packet of N_s bits. The remaining $(N_s - N_p)$ information bits are decoded using the obtained channel estimates. For time $0 < t \leq T_w$, where $T_w = N_w T_f$ and $N_w = N_p N_f$, the received signals correspond to pilot bits and for $T_w < t \leq N_s N_f T_f$, the received signals contain information bits. The received signal over the periods $jT_f \leq t < (j+1)T_f$ for $j = 0, 1, \ldots, N_w - 1$ is

$$r_f^j(t) = b(\lfloor \frac{j}{N_f} \rfloor) \sum_{\ell=1}^{L} \alpha_l p(t - jT_f - \tau_l) + w(t). \quad j = 0, 1, \ldots, N_w - 1 \qquad (3.6)$$

If the transmitters and receivers are asynchronous, an additional time offset term is needed in the above equation but this complication will be investigated in Chapter V.

3.1.3 Channel Estimation

In this subsections, the channel estimation and two detection approaches mentioned above are described. To explain the process of the channel estimation, consider the received pilot waveform in (3.6) for $j = 0, 1, 2, \ldots, N_w - 1$, where α_ℓ and τ_ℓ are the

channel parameters that need to be estimated. In order to use compressed sensing, a sparse representation of signals in a certain basis is desired. One way to achieve this goal is to generate a set of vectors obtained by shifting the pulse function $p(t)$ by integer multiples of a minimum step Δt: $d_j(t) = p(t - j\Delta t), j = 0, 1, 2, \ldots, N_D - 1$. The functions $d_j(t), j = 0, 1, 2, \ldots, N_D - 1$ in the generated basis (or so-called dictionary) $\mathcal{D} = \{d_0(t), d_1(t), d_2(t), \ldots, d_{N_D-1}(t)\}$ are projected with i.i.d. Gaussian random projection $\phi_i(t), i = 1, 2, \ldots, K$ to obtain the projected vectors $\mathbf{v}_j = \int \Phi(t) d_j(t) dt, j = 0, 1, 2, \ldots, N_D - 1$. Denote $\Phi(t) = [\phi_1(t) \ \phi_2(t) \ \cdots \ \phi_K(t)]^T$. The CS channel estimator projects the frame-long received signals $r_f^j(t)$ onto the vectors $[\phi_1(t) \ldots \phi_K(t)]^T$ to obtain $\mathbf{y}_f^j = \int_0^{T_f} \Phi(t) r_f^j(t) dt = [y_f^j[1], y_f^j[2], \ldots, y_f^j[K]]^T, \ j = 1, 2, \ldots, N_w$. Then, an average over all the N_w frames of received signals is used to obtain $\mathbf{y} = 1/N_w \sum_{j=0}^{N_w-1} \mathbf{y}_f^j$. The matching pursuit (MP) algorithm is used to recover the estimate of the multipath channel as shown in Figure 3.2. Notice that the random projection in the analog domain is performed by a set of K synchronized high speed analog mixers that are sampled at the frame rate instead of the pulse rate. The reason to average over all the received signals before processing by the MP algorithm is to reduce the computation cost and noise impact [27]. The MP algorithm chooses one vector which achieves the maximum correlation with $\mathbf{y}$ among all the projected vectors $\mathbf{v}_j$. In other words, in each iteration, MP selects $\mathbf{v}_\ell$ such that

$$\mathbf{v}_\ell = \arg\max_{\mathbf{v}_j} \frac{|\langle \mathbf{y}, \mathbf{v}_j \rangle|}{\|\mathbf{v}_j\|} \tag{3.7}$$

and updates the inner product computed above and the index ℓ as follows:

$$\hat{\theta}_\ell = \hat{\theta}_\ell + \frac{\langle \mathbf{y}, \mathbf{v}_\ell \rangle}{\|\mathbf{v}_\ell\|^2} \tag{3.8}$$

The detailed procedures after the MP algorithm is as follows. Suppose after T_0 iterations, $\hat{\Theta} = [\hat{\theta}_1, \hat{\theta}_2, \ldots, \hat{\theta}_{N_D}]^T$ is a sparse vector obtained from the MP algorithm. Then,

$g_{cs}(t) = \sum_{i=1}^{N_D} \hat{\theta}_i d_{i-1}(t)$ is the estimate of $h(t)$. Let $\hat{\theta}_{(i)}$ for $i = 1, 2, \ldots, N_D$ be the sorted elements of the set $\{|\hat{\theta}_1|, |\hat{\theta}_2|, \ldots, |\hat{\theta}_{N_D}|\}$ and define: $\hat{\theta}_{(1)} = \max\{|\hat{\theta}_1|, \ldots, |\hat{\theta}_{N_D}|\}$, $\hat{\theta}_{(N_D)} = \min\{|\hat{\theta}_1|, \ldots, |\hat{\theta}_{N_D}|\}$, and $\hat{\theta}_{(i_1)} \geq \hat{\theta}_{(i_2)}$ for $i_1 \leq i_2$. Moreover, define $\ell_{(i)}$ as the index in the sparse vector of the ith sorted element, that is $\hat{\theta}_{(i)} = |\hat{\theta}_{\ell_{(i)}}|$. The estimated path gain and path delay for the ith propagation path are

$$\hat{\alpha}_i = \hat{\theta}_{\ell_{(i)}}$$

$$\hat{\tau}_i = (\ell_{(i)} - 1)\Delta t \tag{3.9}$$

for $i = 1, 2, \ldots, L_c$, where L_c is the number of the paths that are considered and Δt is the same parameter for the minimum time shifting of the transmitted pulse $d_j(t) = p(t - j\Delta t), j = 0, 1, 2, \ldots, N_D - 1$.

3.1.4 CS Rake Receiver

For the CS rake receiver, the received signal $r(t)$ is correlated with a bank of correlators with the shifted pulses $p(t - \hat{\tau}_i)$ for $i = 1, 2, \ldots, L_c$. The outputs of these correlators are combined by maximum ratio combining (MRC) with corresponding $\hat{\alpha}_i$ to form a sufficient statistic to detect the kth transmitted bit in the jth frame. The result is

$$z_R(k, j) = \sum_{\ell=1}^{L_c} \hat{\alpha}_\ell \int_{kT_b+jT_f+\hat{\tau}_\ell}^{kT_b+jT_f+\hat{\tau}_\ell+T_p} r(t)p(t - kT_b - jT_f - \hat{\tau}_\ell)dt. \tag{3.10}$$

Observe that the energy of the received signal is identified by correlating the received signal with L_c shifted versions of the transmitted pulses and a frame rate sampling frequency is required to perform correlation and weighted combination. Since one bit of information is transmitted by N_f frames, the detection of the kth transmitted bit is expressed as follows:

$$\hat{b}(k) = \text{sgn}\left(\sum_{j=0}^{N_f-1} z_R(k, j)\right). \tag{3.11}$$

23

Note that in the previous discussion, it is assumed that the number of "fingers" in
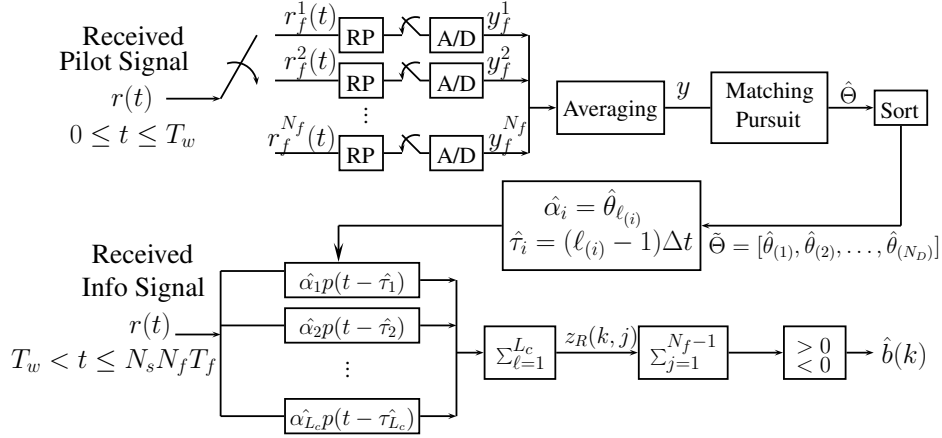
Figure 3.2: Scheme Ia: CS rake receiver

the bank of correlators is equal to the number of strongest paths L_c. In a practical scenario, the choice of the number of fingers is a tradeoff between performance and complexity. Furthermore, the number of the MP iterations T_0 should be greater than the number of fingers so that in the process of the MP, the path selected in the previous iterations of the MP can be updated. The complexity of the channel estimation is mainly determined by the MP algorithm, whose complexity is approximately $\mathcal{O}(CL_cT_0)$, where C is a constant depending on the size of the dictionary. The whole structure of CS rake-based detector is shown in Figure 3.2. Beside MP algorithm, the spectral projected-gradient (SPGL1) recovery algorithms is used to obtain the channel template in the simulation. The SPGL1 algorithm is one kind of basis pursuit (BP) algorithm, which is optimized in the ℓ_1-norm sense instead of ℓ_2-norm sense in the MP algorithm.

3.1.5 CS Correlator-Based Detector

As in the CS rake receiver, the correlator-based detector in Figure 3.3 uses MP to recover a noisy template of the multipath channel as expressed in (3.3) by considering a frame-long period of the signal and randomly projecting the signal with the random

projection operator $\Phi(t)$. The difference is that it is not needed to sort $\hat{\Theta}$, but simply use $g_{cs}(t)$ as the channel template to correlate with the received information signal to perform demodulation with frame rate sampling. The detection statistics for the kth
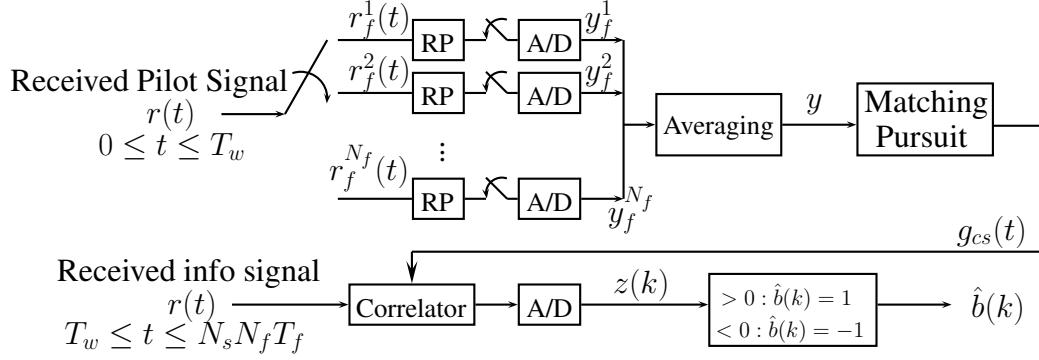
Figure 3.3: Scheme IIa: CS correlator receiver

bit is composed of N_f correlator output samples related to the transmitted symbol:

$$z(k) = \sum_{j=0}^{N_f-1} \int_{jT_f+kT_b}^{(j+1)T_f+kT_b} r(t)g_{cs}(t - jT_f - kT_b)dt \qquad (3.12)$$

One can also extend this frame rate sampling detector to a symbol rate detector by repeating the template $g_{cs}(t)$ N_f times every T_f seconds, correlating this symbol-long template with received signals, and sampling the correlator output at the symbol-rate to detect the transmitted signal.

3.1.6 Alternative Receiver Structures

Improving upon the correlator and rake receiver structures introduced in [27] and in the above subsection, other receiver structures are presented in this section. First, the diagrams of the projection processes in Figure 3.2 and 3.3 are simplified into one block in Figure 3.4 since the focus is on the whole structure. The CS rake receiver is categorized as scheme I and CS correlator receiver is scheme II and the original structure is further classified as Type a. Following this, the above rake receiver is
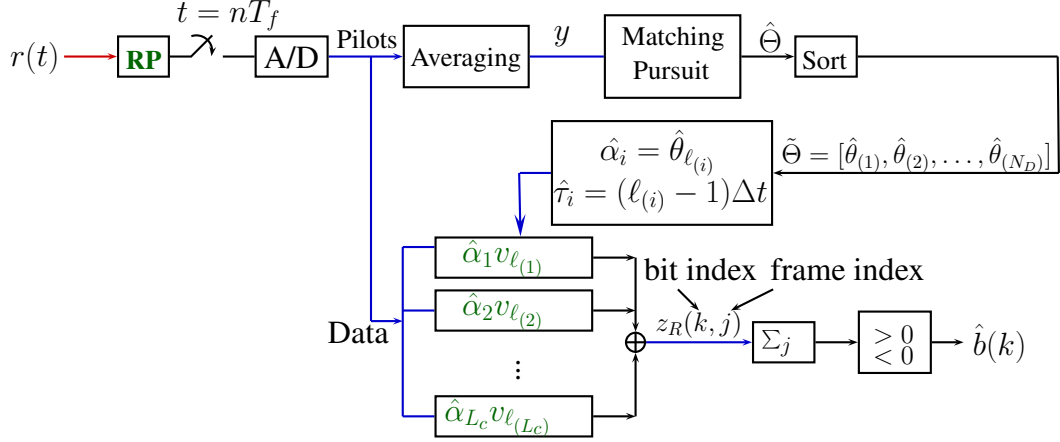
Figure 3.4: Scheme Ib: CS rake receiver with random projection on pilot and info signals

called as scheme Ia and the correlator receiver in Figure 3.3 is labeled as scheme IIa. Scheme Ib shown in Figure 3.4 is a modification of the receiver scheme Ia. Notice that, in scheme Ib, both the received pilot and information signals are processed by a projection matrix. Under this new structure, the dimension of the received signal is reduced and the possible requirement of a high sampling rate is avoided in detection. Note that the received projected information signal is correlated with the projected vectors $\mathbf{v}_j = \int \Phi(t) d_j(t) dt, j = 1, 2, \ldots, N_D$ as stated in section 3.1.3. The correlating process in each finger of the rake receiver in the compressed projected dimension is called smashed filtering whereas the correlating process in that of the rake receiver in original signal space as in scheme Ia is called matched filtering.

Another structure that can be obtained by simply substituting the random projection matrix with a Hadamard matrix is called scheme Ic and is shown in Figure 3.5. In this way, the complexity of implementation of doing a projection with a Gaussian vector is reduced. Similarly, these two new structures can also be adopted in a CS correlator and are called scheme IIb and IIc, as shown in Figure 3.6 and Figure 3.7. In the both figures, $\hat{s}_\phi = \sum_{i=1}^{N_D} \hat{\theta}_i \mathbf{v}_{i-1}$, which is the estimated template in the reduced domain.
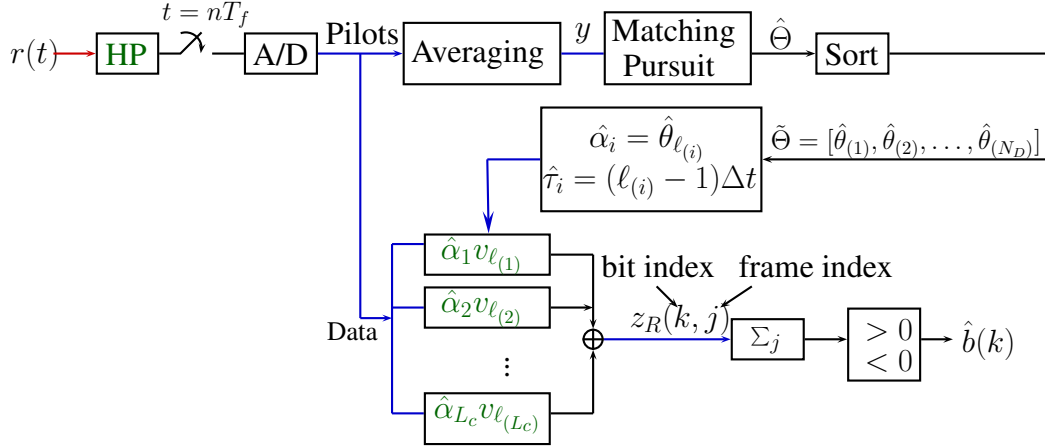
Figure 3.5: Scheme Ic: Rake receiver with Hadamard projection on pilot and info signals
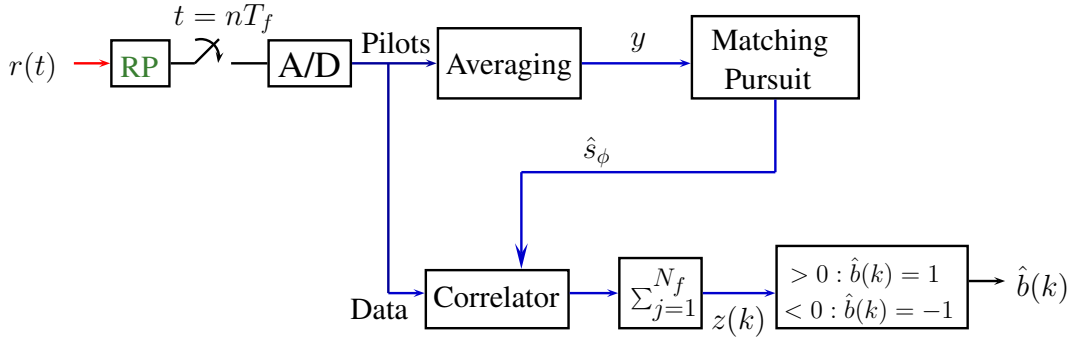
Figure 3.6: Scheme IIb: Correlator receiver with random projection on pilot and info signals
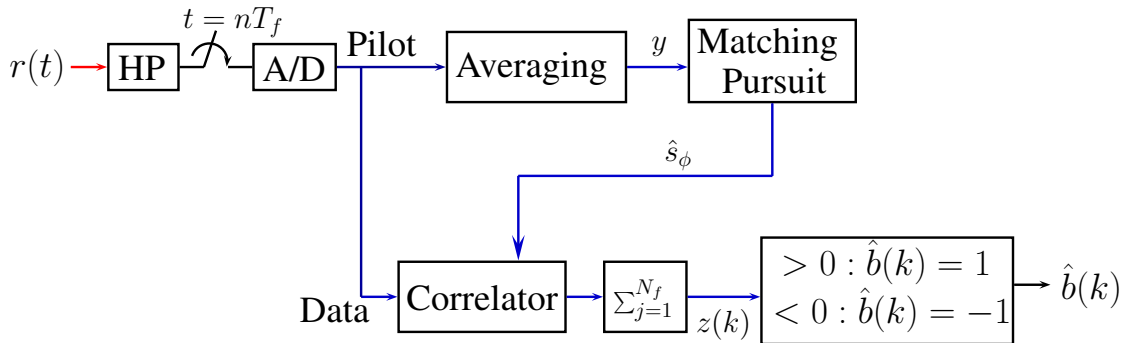
Figure 3.7: Scheme IIc: Correlator receiver with Hadamard projection on pilot and info signals

To compare the performance of the CS-correlator and the CS-Rake, the conventional correlator-based detector is constructed by averaging all the received wave-
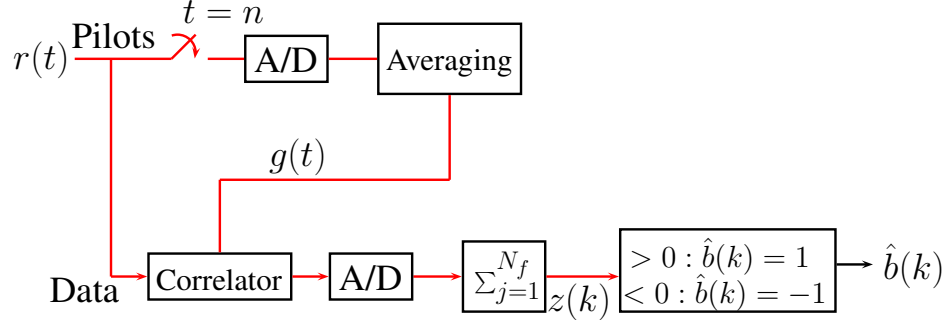
Figure 3.8: Scheme IIIa: Conventional correlator receiver

forms: $g(t) = \sum_{j=0}^{N_w - 1} r_f^j(t)/N_w$, where $r_f^j(t)$ is given by (3.6). Figure 3.8 shows this structure. The above structure is further modified by processing the received signals with a random projection matrix to reduce the dimension of the signal and implementation complexity. The resulting structure is shown in Figure 3.9. Moreover,
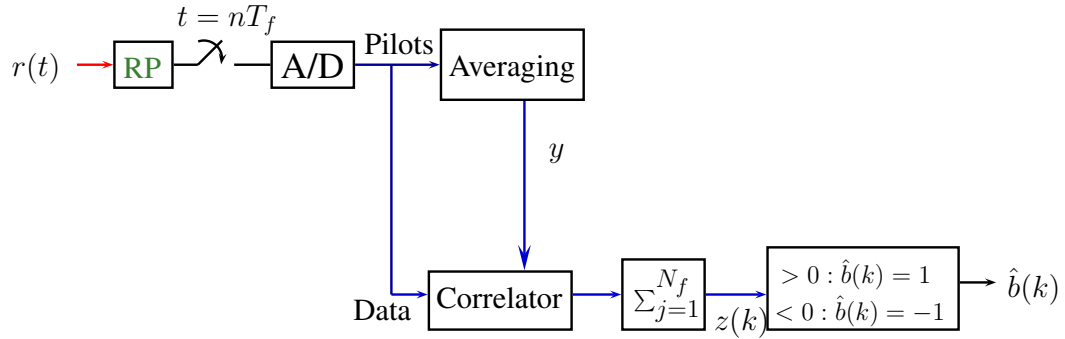
Figure 3.9: Scheme IIIb: Conventional correlator receiver with random projection on pilot and info signals

the random projection matrix with the Hadamard matrix is substituted to further simplify implementation and label this as scheme IIIc as demonstrated in Figure 3.10. Table 3.1 shows the different receiver structures categorized in different schemes and types.
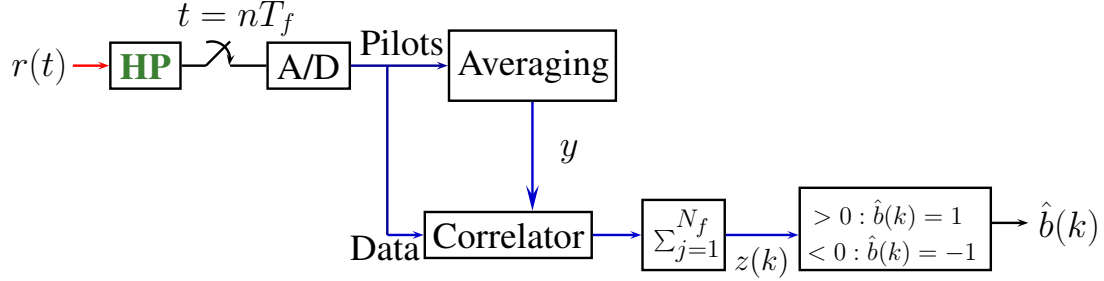
Figure 3.10: Scheme IIIc: Conventional correlator receiver with Hadamard projection on pilot and info signals

	Scheme I	Scheme II	Scheme III
Type a	CS Rake matched filter	CS Correlator matched filter	Conventional Correlator matched filter
Type b	CS Rake smashed filter,RP	CS Correlator smashed filter,RP	Conventional Correlator smashed filter,RP
Type c	CS Rake smashed filter,HP	CS Correlator smashed filter,HP	Conventional Correlator smashed filter,HP

Table 3.1: Different receiver structures

3.2 Simulation Results

3.2.1 No Quantization

The standard IEEE 802.15.4a [24] is chosen as the multipath channel model in the simulation. In the standard, the power delay profile is described in the similar form as in (3.3). The τ_ℓ in (3.3) is a poisson process and $E(|\alpha_\ell|^2)$ is exponential. The performance criterion is the bit error rate (BER) as the function of signal-to-noise ratio (SNR), which is defined as E_b/N_0, where E_b is the received energy per bit $(E_b = \int_t \left(\int_\tau h(t-\tau)p(\tau)d\tau \right)^2 dt)$ and $N_0/2$ is defined as the power spectral density of AWGN. The first derivative of the Gaussian pulse is the transmitted pulse $p(t)$, which is normalized to unit energy and has duration 0.65ns. The frame duration T_f is set to be 100ns and the number of frames N_f in one bit is 25. Moreover, PAM is used in the simulations and $b(k)$ is independent and having equal probability of being +1 and -1 . The sampling frequency before projection is set at 20GHz and

Δt is set equal to one sampling period, 50ps. The sampling frequency 20GHz is considered as the time resolution of the simulation and only used for simulation but not in actual implementation. For example, considering one frame of the kth bit received signal $r_{f,k}(t)$ as defined in (3.4), it is sampled to obtain the discrete-time vector $\mathbf{r_f} = [r(0)\ r(T)\ \cdots\ r((N-1)T)]^T$, where T is 50ps. Moreover, define $\mathbf{y} = \Phi \mathbf{r_f}$ as the random projected received signal where Φ is a $K \times N$ measurement matrix with each element $\phi_{i,j} \sim \mathcal{N}(0,1)$, where $N = 2000$. Then the MP [21] algorithm is applied on the random projected received signal $\mathbf{y}$ to estimate the multipath channel. Moreover, the negligible tail of the multipath impulse response is cut off to set the maximum delay spread equal to 99.35ns, which plus a pulse duration, 0.65ns, is equal to 100ns, the same as T_f so that there is no intersymbol interference. The remaining energy of the channel impulse response is normalized to one. The BER performance is evaluated over the same "random" generated channel but with different noise and estimate this channel 50 times to generate a smooth curve. For each estimation of the channel, $N_s = 10000$ bits are transmitted, N_p of these bits are used as pilot bits to estimate the channel and reconstruct the template for detecting the following 10000-N_p information bits. The BER is calculated by averaging the BER obtained for each channel estimation. Hence, for each channel realization, $50 \times (N_s - N_p)$ bits of information are transmitted.

The parameters used in matching pursuit algorithm are set in the following description. The number of iterations T_0 is 400 and the target residual error is $\epsilon_0 = 10^{-4}$. There are $L_c = 50$ fingers in the rake receiver used to correlate with the received signal. In Figure 3.11, the BER performance of the 3 detection schemes, Scheme Ia, IIa, and IIIa for the different number of pilot bits N_p is shown. In the simulation, the number of measurements K is 720. As shown in Figure 3.11 and 3.12, increasing number of pilot bits improves the channel estimation and thus has better performance for all the 3 detection schemes. At the expense of a slight loss in transmitted energy to estimate
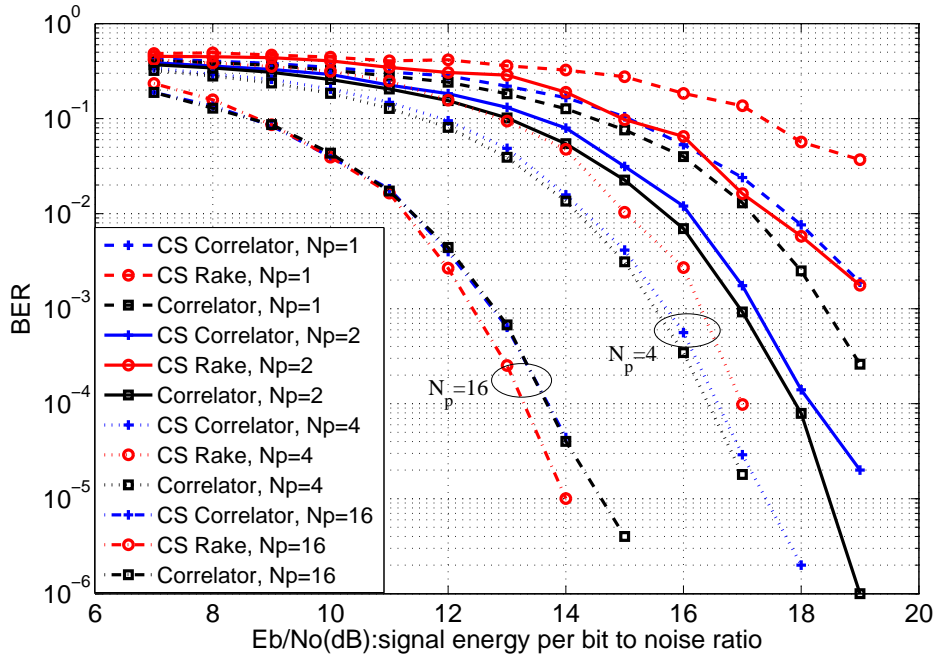
Figure 3.11: BER performance for different number of pilot bits N_p=1, 2, 4, 16, with K =720
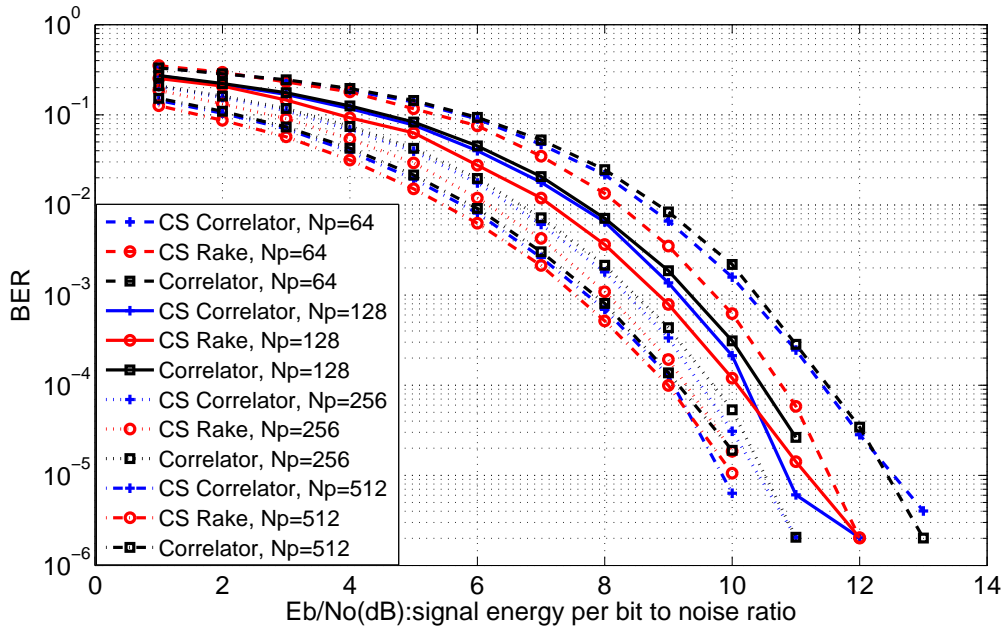
Figure 3.12: BER performance for different number of pilot bits N_p=64, 128, 256, 512, with K=720

the channel, the BER performance improves significantly. If the number of pilot bits is increased up to 512 as shown in the Figure 3.12, the BER performance approaches the case where a perfect channel template is used and is roughly with $BER = 10^{-5}$ at SNR=9.6(dB). The energy in pilots is not take into account while plotting the BER v.s. E_b/N_0 figure.
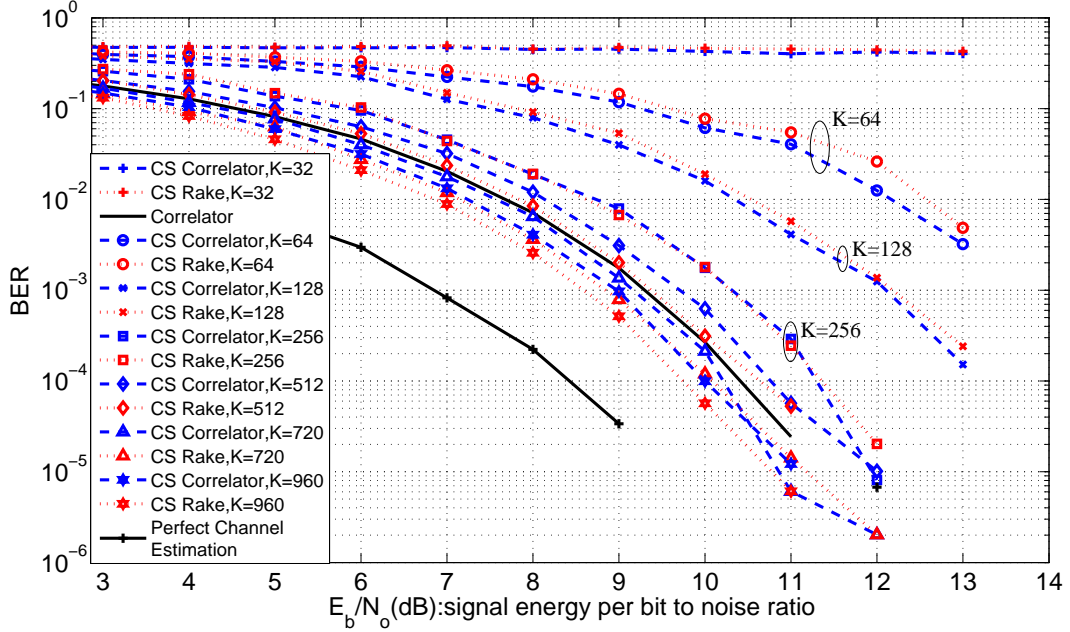
Figure 3.13: BER performance for different number of projection K=32, 64, 128, 256, 512, 720, 960, and perfect channel estimations with N_p=128

In Figure 3.13, the BER performance of the Scheme Ia, IIa, and IIIa for different number of projections is demonstrated. It is interesting to note that the performance of CS-rake becomes better than that of CS-correlator when $K > 256$, which can be explained as follows. As number of projection K increases, the reconstruction of the channel template is more accurate so even if there are only L_c=50 fingers in my detector, these first 50 largest components already capture the main energy of the whole signal. On the other hand, although CS-Correlator use more than 50 elements in the dictionary to form the estimated channel template, it may contain

32

more incorrectly identified elements to represent the channel estimation and result in the worse performance. Figure 3.14 shows the BER performance when the
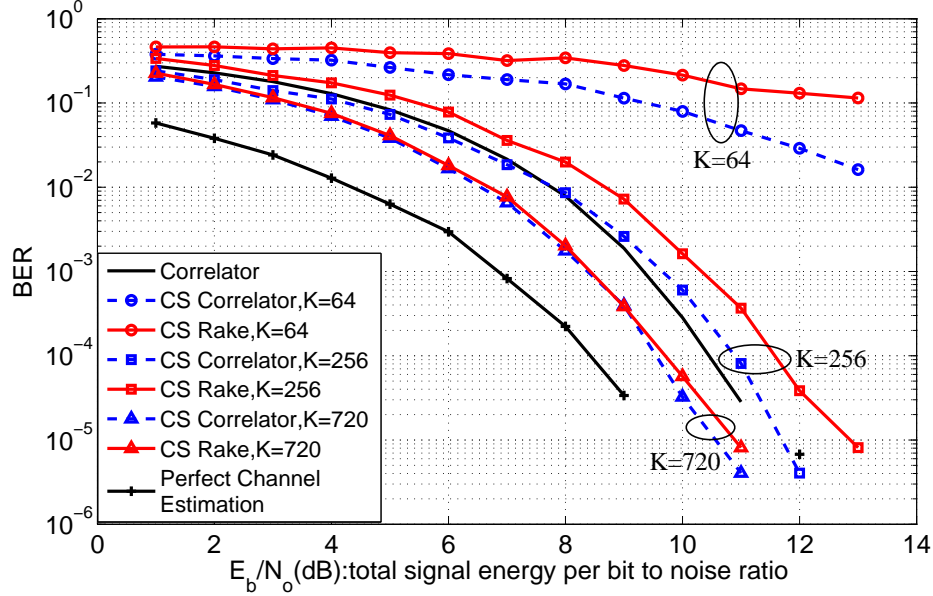
Figure 3.14: BER performance for using Hadamard matrix K=64, 256, 720, with N_p=128

random projection matrix is replaced with the Hadamard matrix. The performance is comparable to that while using random projection matrix, especially in the case with higher K. In this case, CS-correlator outperforms CS-rake at lower K. At K=720, the performance of these two receivers are almost the same and are both better than the conventional correlator-based receiver.

In Figure 3.15, the BER performance is compared among different schemes with a repetition code. The performance of the receivers with Hadamard matrices (Type c) is superior to that with random matrices (Type b). The conventional correlator-based receiver (Type a) represented by the black line have 2dB gain in E_b/N_0 but requires much higher sampling rate as pointed out previously.

The BER performance among different schemes with Hadamard coding is shown in Figure 3.16. It can be observed that the performance is better than those with
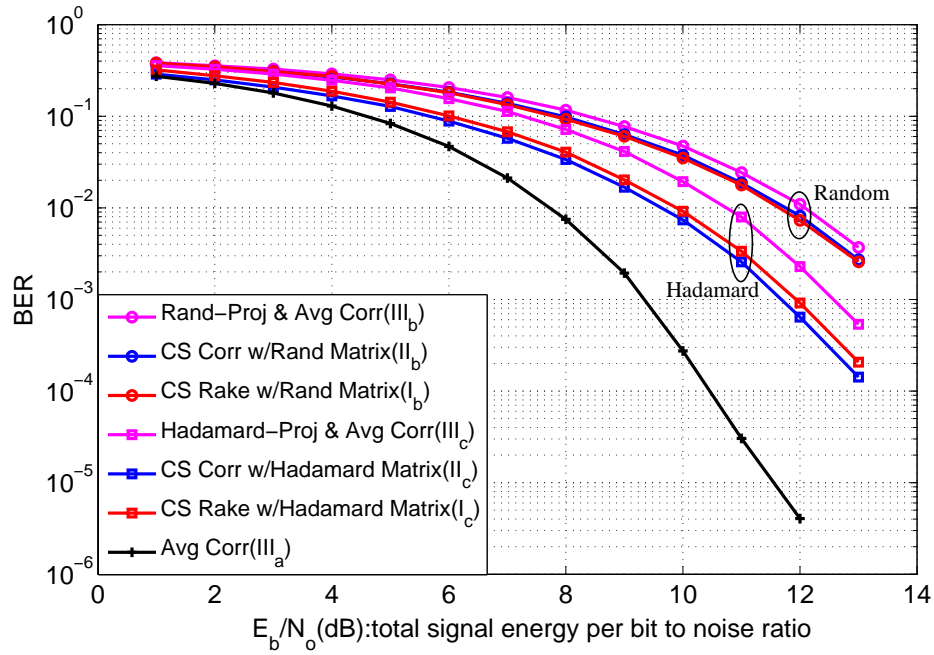
Figure 3.15: BER performance compared among different schemes, N_f=25, repetition code, K=720, N_p=128
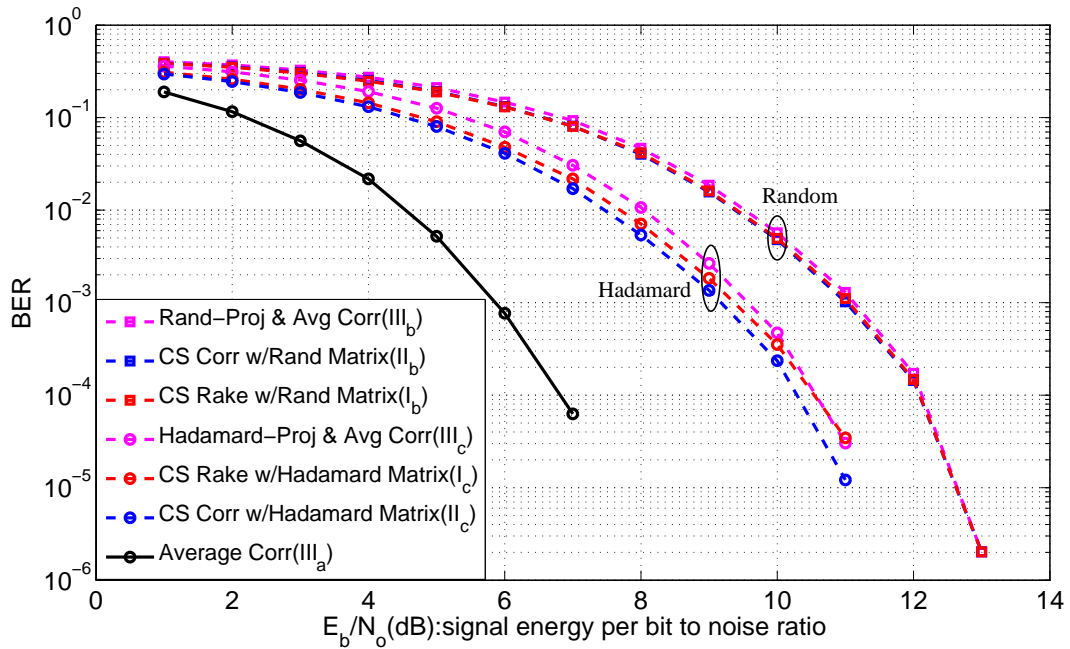
Figure 3.16: BER performance compared among different schemes, N_f=32 Hadamard Code, K=720, N_p=128

repetition code by the coding gain. The performance of the receivers with Hadamard matrices (Type c) still outperforms those with random matrices (Type b). With the same type, the performances of the receivers with different schemes are almost equal. The conventional correlator-based receivers (Type a) shows 3dB gain but requires more than one hundred times the sampling rate, increasing from $1/T_f = 1/100(ns) = $ 10 MHz to $1/T_p = 1/0.65(ns) \approx 1.54$ GHz.

3.2.2   Impact of Finite Bit Quantization

In the previous sections, the signal values are assumed to be processed with very high resolution in our system model. In this section, I investigate the effect of the bit quantization on channel estimation by comparing the BER performance of the receiver without quantization and the ones with different numbers of bits in quantization resolutions. Some simulation parameters are changed as follows to accommodate the circuit design specification. The simulation sampling time resolution is 0.625ns. The number of samples in one frame denoted by N is changed to 64 so the frame duration T_f is 39.375ns ($0.625 \times (64-1)$) and the square pulse shape is used with values 0 and 1 and the duration T_p=1.3ns is used.

3.2.2.1   Perfect Channel Estimation

To generate the waterfall curves, assuming an ideal channel with AWGN noise, two different receiver architectures were considered, both based on matched filtering as shown in Fig. 3.17. In the first architecture, compressed samples are taken in the Hadamard domain and the time domain sparse signal is recovered using spectral projected-gradient (SPGL1) which is then correlated with an ideal template to make bit decisions. In the second architecture, the difference is that matched filtering is done directly in the Hadamard domain using sub-Nyquist samples (also known as smashed filtering in the CS literature) rather than in the time domain after recon-

struction.
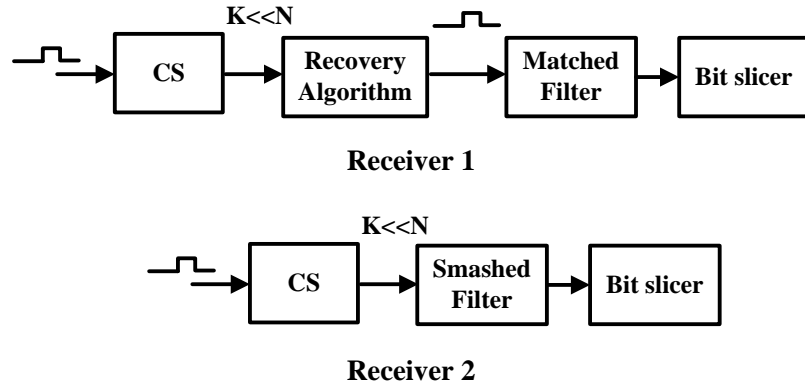
Figure 3.17: Receiver architectures for waterfall curves
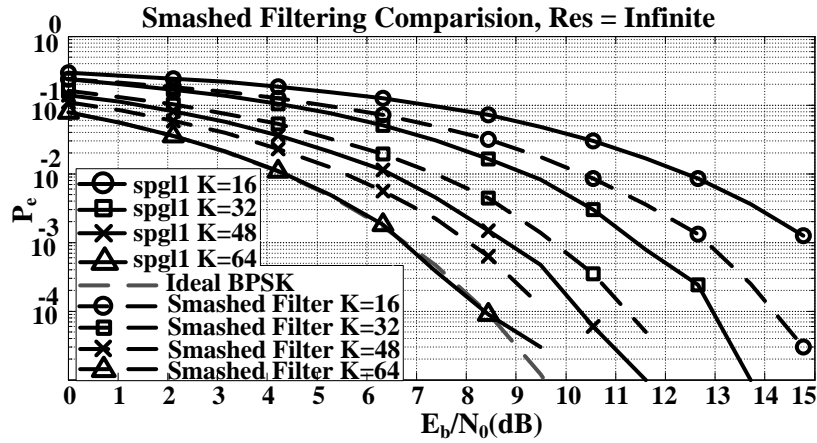
Figure 3.18: BER curves for infinite resolution

Figure 3.18 shows the BER curves for both receiver architectures for infinite reso-lution of the sub-Nyquist ADC and compares it with an ideal BPSK curve for different values of K. It is found that the smashed filter has better performance compared to the matched filter in the time domain. One explanation for this is that the recovery algorithm attempts to find a sparse solution in the time domain to a given set of compressed measurements K. However, a signal with low SNR cannot be considered sparse, because noise produces many non-zero values. The recovery algorithm in the CS framework assumes a sparse solution to the given set of compressed measure-
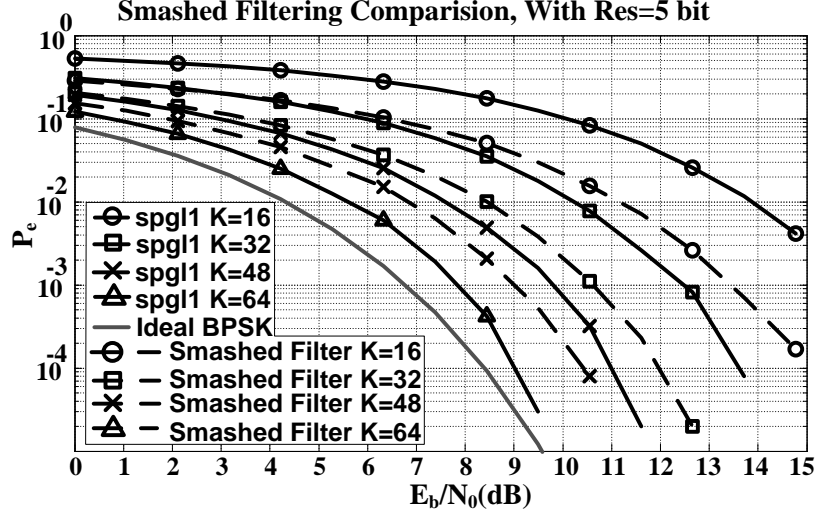
Figure 3.19: BER curves for Res=5bit

ments. As a result, the algorithm attempts to reconstruct the noise with the sparse solution. This affects the performance of the matched filter and results in an increased probability of error (P_e) at a given signal-to-noise ratio (E_b/N_0) for $K < N$.

Figure 3.19 shows the BER curves for 5 bit resolution of the sub-Nyquist ADC quantizing Hadamard coefficients. In this case the BER curve for $K = N = 64$ does not overlap the ideal BPSK curve due to the quantization noise.

3.2.2.2 Multipath Channel Estimation

In this subsection, the IEEE 802.14.4a standard channel model is also used in the simulation on the multipath channel estimation. It should be pointed out that the BER performance of the receivers in Figures 3.20, 3.21, 3.22, 3.23, 3.24, and 3.25 are for smashed filtering and in Figures 3.26 and 3.27 are for matched filtering. Figure 3.20 to 3.23 discussed below are with a fixed number of fingers L_c=50 in the CS rake receiver and a fixed number of pilot bits N_p=128. The following simulation figures are focused on smashed filtering since with perfect channel estimation it is found to be better than matched filtering. The BER performance is shown in Figure 3.20, where
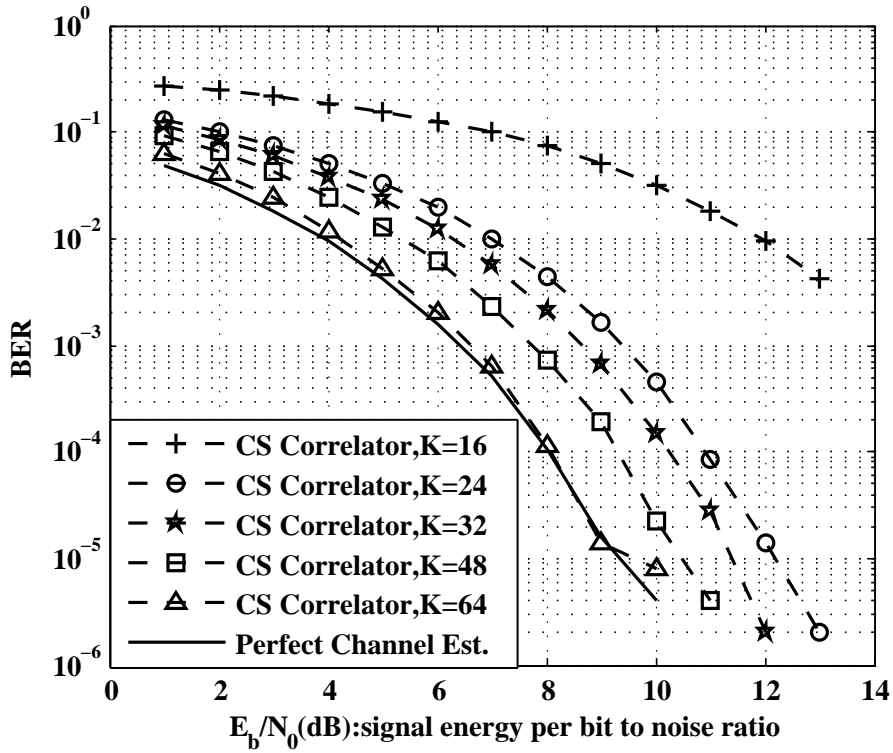
Figure 3.20: BER Performance for different number of projected measurement K=16, 24, 32, 48, 64, no quantization, smashed filter, SPGL1. The BER curves for CS rake and correlator are nearly identical to that of CS correlator

the receiver without quantization for different values of K is evaluated when using the smashed filter to correlate the received signal with a noisy estimated channel template. The waterfall curves show that the BER performance is improved when K is increased, as expected.

Figure 3.21 shows the BER performance of the smashed filter for different quantization resolutions with a fixed K=24. It is observed that there is 2 dB gap between 1-bit and 3-bit quantization resolution but beyond 5-bit resolution, the improvement is insignificant. This 2 dB gap conforms to the common knowledge that the performance of a hard decision detector is often $2 \sim 3$ dB worse than that of a soft decision detector. The receiver with 1-bit quantization resolution is essentially a hard decision detector and the receiver with 5-bit quantization is very close to an ideal soft deci-
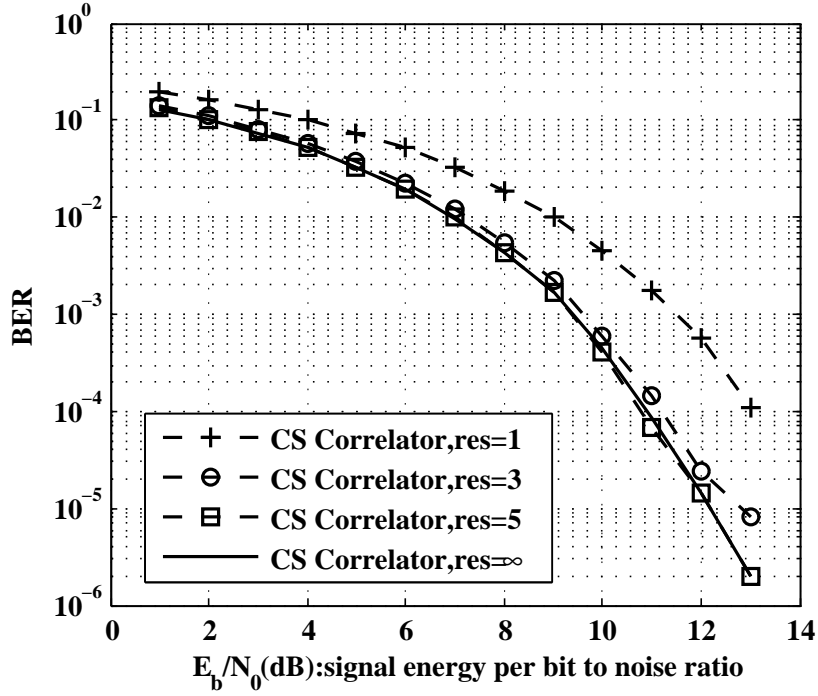
Figure 3.21: BER performance for the smashed filter with different number of bit resolution: $1,3,5,\infty$, with $K{=}24$, SPGL1. The BER curves for CS rake and correlator are nearly identical to that of CS correlator

sion detector. Therefore, in Figure 3.22, the quantization resolution is fixed at 5 bits and the value of K is varied. It shows again that the BER performance is improved through increasing the number of K, as expected.

Next, instead of using the SPGL1 algorithm to estimiate the channel, the MP algorithm is applied to recover the multipath channel template in the receiver. The comparison between the receivers with SPGL1 and MP algorithm is shown in Figure 3.23. The performance of MP is similar to the previous case using the SPGL1 algorithm. The larger the K is used in the receiver, the better the performance shows. Figure 3.23 shows the excess E_b/N_0 needed to achieve $P_e = 10^{-3}$ versus K/N of 4 different receivers with quantization resolution of 5-bits or without quantization and using the MP or SPGL1 algorithm. It is interesting to notice the significant drop of
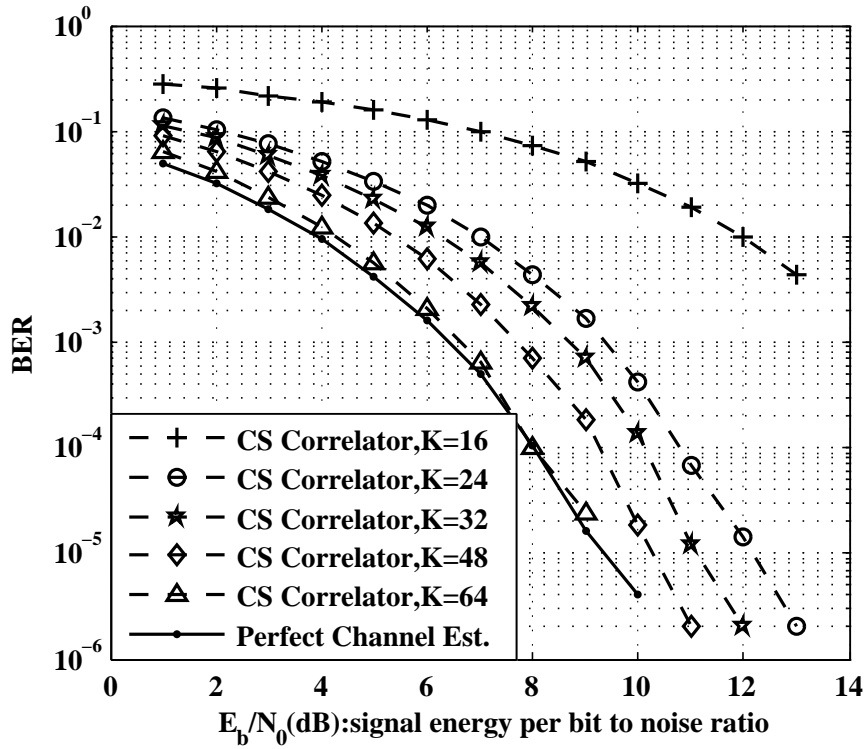
Figure 3.22: BER Performance for different number of projected measurement K=16, 24, 32, 48, 64, with quantization resolution=5 bits, smashed filter, SPGL1. The BER curves for CS rake and correlator are nearly identical to that of CS correlator

excess E_b/N_0 as K/N varies from 25% ($K = 16$) to $K/N = 37.5\%$ ($K = 24$). It is also observed that the 4 curves are nearly identical.

Figure 3.24 shows the BER waterfall curves with different values of N_p and fixed L_c=50. It is observed that the 3 different receiver structures (CS correlator, CS rake, and correlator) have almost the same performance for each value of N_p. For simplicity, 3 different structures are shown only for $N_p = 1$ and only the curves for the CS correlator are shown for $N_p > 1$. On the other hand, Figure 3.25 shows a different phenomenon that by increasing the number of fingers L_c in the rake receiver, the performance improves for the rake receiver while the performance of the other two receivers remains the same, as expected. The curves for the CS correlator are
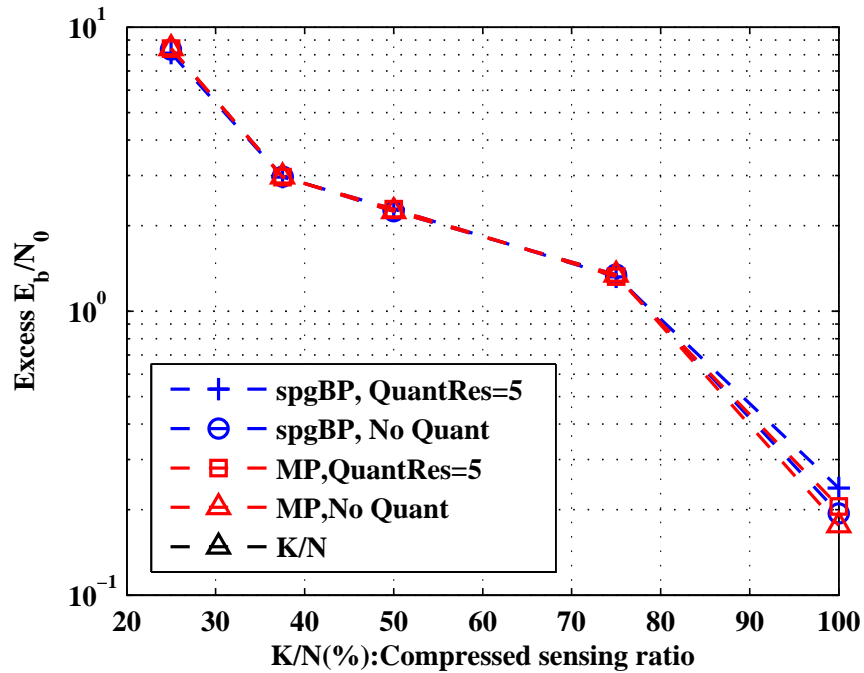
Figure 3.23: Excess E_b/N_0 Required for Different K in Different Receiver Schemes

also omitted for simplicity.

Considering a receiver with a matched filter, Figures 3.26 and 3.27 show the BER performance with different values of N_p while L_c=50 is fixed and various values of L_c while N_p=128 is fixed. Notice that the performance of L_c=2 is quite close to that of L_c=50, when N_p=128 is fixed. On the other hand, when L_c is fixed at 50, increasing the number of pilot bits gradually improves the performance without any large jumps.

3.3   Conclusion

In this chapter, the channel estimation in UWB system using compressed sensing is introduced. The procedure using MP algorithm to estimate a multipath channel is described and the estimated channel template is exploited to detect transmitted information bits. The different receiver structure and coding scheme are also presented to reduced the complexity of computation in the system and obtain coding gain in
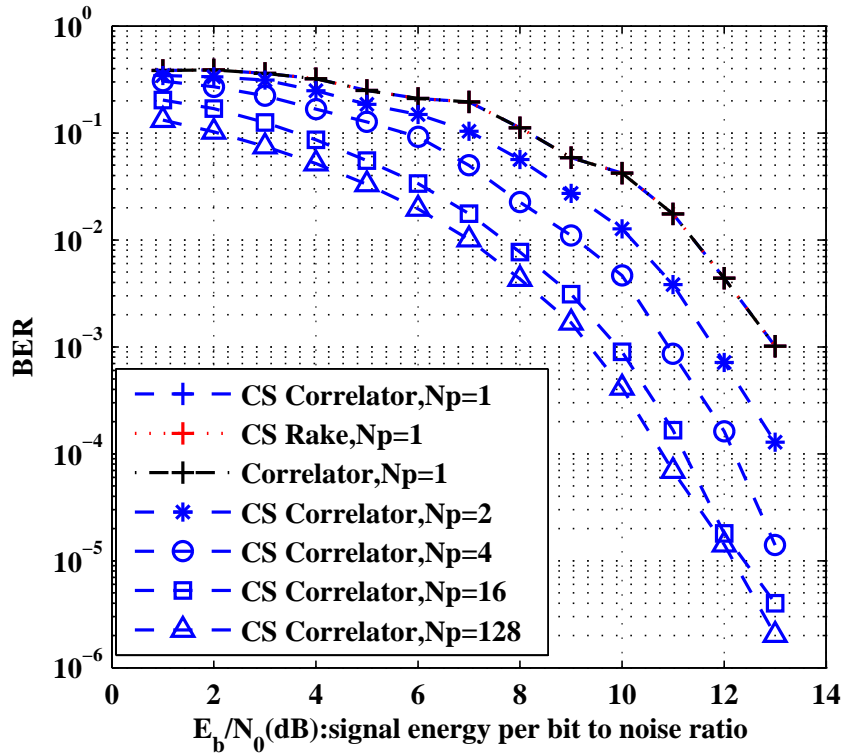
Figure 3.24: BER Performance for different number of pilot bits N_p=1,2,4,16,128, with K=24, L_c=50, smashed filter, SPGL1. The BER curves for CS rake and correlator are nearly identical to that of CS correlator.

BER performance. In simulation, the BER performance without quantization is first illustrated with different numbers of projection K, different number of pilot bits N_p, and different receiver schemes and types. The impact of finite bit resolution is then investigated with different numbers of projection, pilot bits, and different numbers of fingers used in the rake receiver.

To sum up, one can observe that the BER performance with 3-bit resolution is comparable to that with infinite bit resolution. The number of projection K=24 out of N=64 also yield the performance close to that with K=64. The number of pilot N_p=16 produces similar performance to N_p=128. The smashed filtering loses 3 dB in SNR at the same BER compared to the matched filters. These results provide a guideline for choosing related system design parameters.
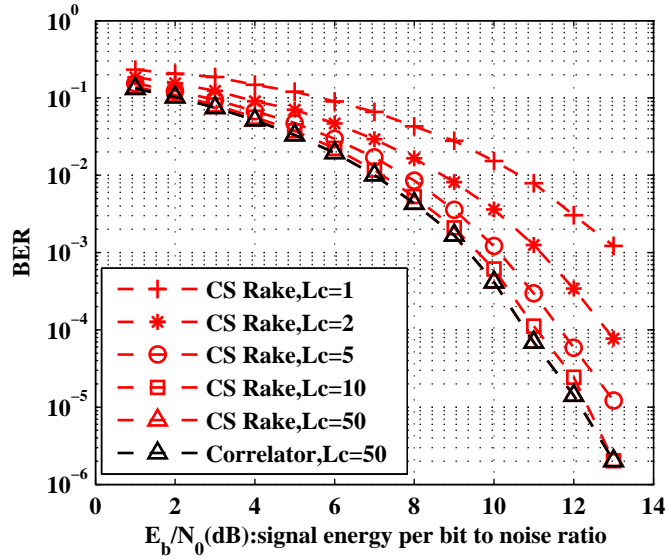
Figure 3.25: BER Performance for different number of fingers in rake receiver L_c=1, 2, 5, 10, 50, N_p=128, with K=24,quantization resolution=5 bits, smashed filter, SPGL1. The BER curves for correlator are nearly identical to that of CS correlator.
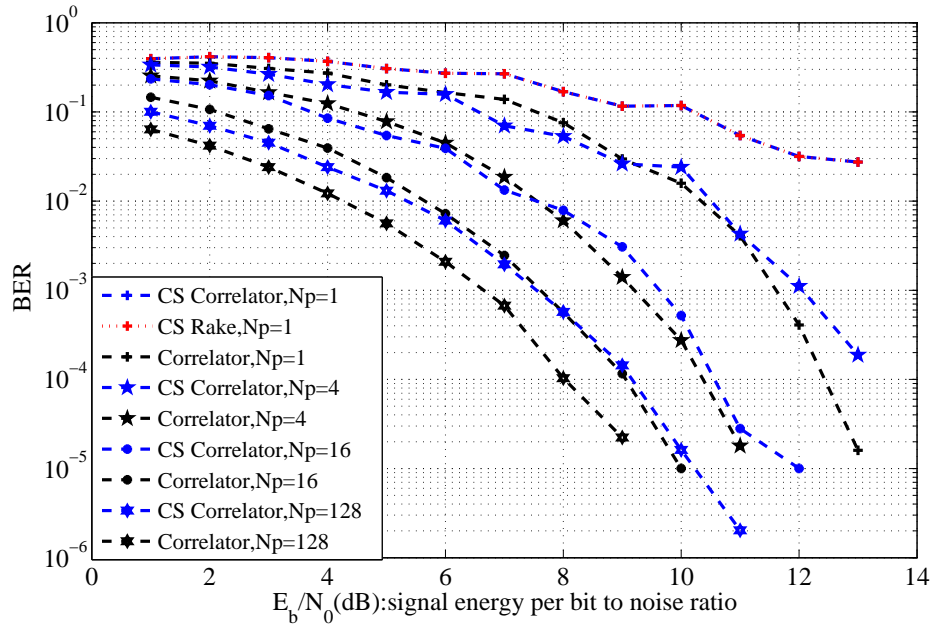
Figure 3.26: BER Performance for different number of pilot bits $N_p = 1, 4, 16, 128$, with L_c=50, K=24, quantization resolution=5 bits, SPGL1. The BER curves for CS rake are nearly identical to that of CS correlator.
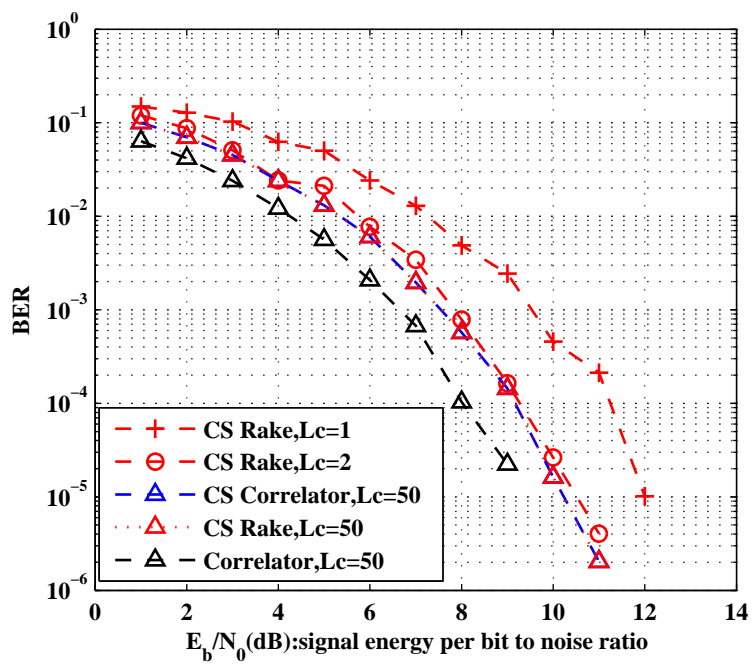
Figure 3.27: BER Performance for different number of fingers L_c=1, 2, 50 in Rake receiver, with K=24, quantization resolution=5 bits, SPGL1

CHAPTER IV

Channel Measurement and Channel Capacity

4.1 Introduction

Channel capacity is defined as the least upper bound on the rate of information that can be reliably transmitted over a communication channel. In order to calculate channel capacity, it is essential to have the knowledge of channel characteristic. The IEEE standard 802.15.4a [24] specifies several channel models for ultra-wide band (UWB) systems in different scenarios such as 1) indoor residential, 2) indoor office, 3) industrial environment, 4) body-area network (BAN), 5) Outdoor, and 6) agricultural area/farms. The 5th model only covers a suburban-like microcell scenario. Hence, there is no channel models in IEEE 802.15.4a specifically for sensors located at girders under a bridge, where the sensors are deployed. To understand the fundamental limit of the rate of transmission in a particular scenario, the channel measurement for this specific environment is needed. The channel measurement procedures is described in the following Section 4.2. The theorem used to calculate the channel capacity and the corresponding plots are covered in Section 4.3.

4.2 Channel Measurement

The actual UWB channel response is measured at the site using the PulsON 200 Evaluation Kit (EVK) from the Time Domain Corporation. The antenna of the EVK is shown in Figure 4.1. The transmitted pulses radiated from the UWB antenna

Figure 4.1: A transmitter/receiver in EVK

is presented in Figure 4.2. The measurement is performed under the bridge and the transmitter is fixed at the edge of the bridge width on one side of the Telegraph Road while the receiver is placed at the different girders under the bridge and also on the other side of the road. The actual environment is shown in Figure 4.3. For each measurement, a 110ns waveform is recorded with sampling rate at 31.78 ps as shown in Figure 4.4. The recorded waveforms are used to estimate the channel impulse responses by CLEAN algorithm [16]. The CLEAN algorithm is the same as the matching pursuit (MP) algorithm describe in Section 2.2. The idea is for each iteration, the largest component within the remainder signal vector is chosen by correlating the signal with the vectors in a basis which span the signal space. The corresponding location and amplitude of the largest component is recorded. Then, this largest component is subtracted from the remainder signal and the subtracted vector is compared with specific threshold of the signal energy. If the remaining
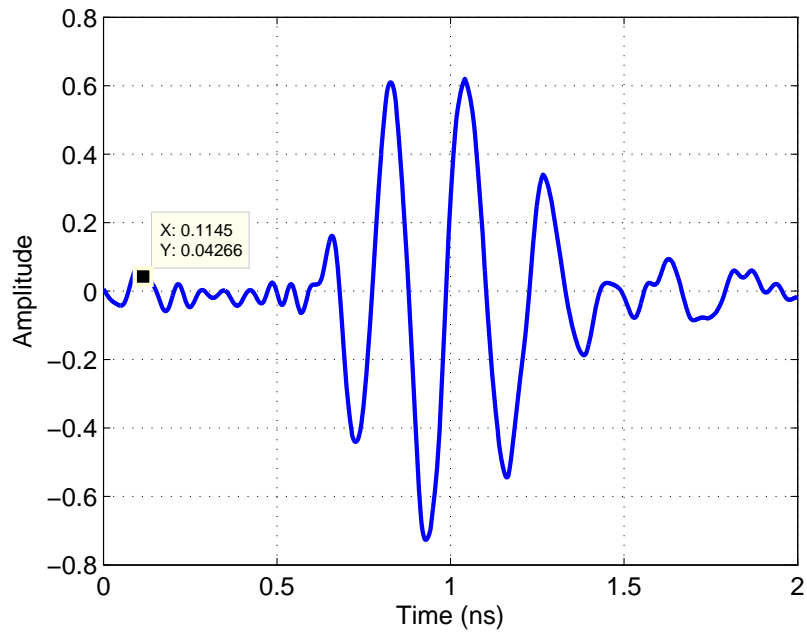
Figure 4.2: A transmitted pulse

Figure 4.3: Measurement environment: the girders under the bridge

energy is smaller than the threshold or the number of iteration is more than certain value, the process is stopped. Otherwise, the procedure continue to find the largest
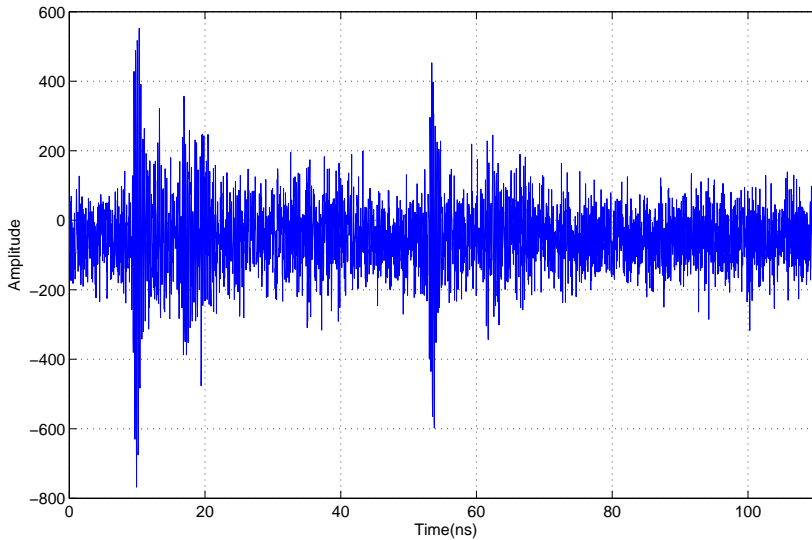
Figure 4.4: A measured waveform at the receiver

component in the remaining signal.

4.3 Channel Capacity and Results

The estimated channel impulse response obtained by the CLEAN algorithm is used to calculate the channel capacity as follows [14]. Recall that the channel model described in (3.3) is a continuous time model. Consider the model in discrete time domain and can be written as the following equation:

$$r_k = \sum_{i=0}^{L-1} h_i s_{k-i} + n_k, \quad -\infty < k < \infty \tag{4.1}$$

where the real transmission sequence $\{s_k\}$ produces the real received sequence $\{r_k\}$ and the finite-length sequence $(h_0, h_1, \cdots, h_{L-1})$, with $h_0 \neq 0$ and $h_{L-1} \neq 0$, is the unit-sample response of the equivalent channel filter. The transfer function of this filter

$$h(\lambda) = \sum_{i=0}^{L-1} h_i e^{-ji\lambda}, \quad j = \sqrt{-1} \tag{4.2}$$

48

is periodic in λ with period 2π.

The authors in [14] define a new channel model by changing (4.1) to the cyclic channel model as:

$$\tilde{r}_k = \sum_{i=0}^{L-1} \tilde{h}_i s_{((k-i))} + n_k, \quad 0 < k < N \tag{4.3}$$

where $((\cdot))$ denotes modulo N and where $N > L$. The reason to define a new model is that in practice, only a finite duration of the received signal is processed at a time in the receiver. Hence, the number of samples N is bounded. Using the notation $\tilde{h}[0, N-1] = (h_0, h_1, \cdots, h_{L-1}, 0, 0, \cdots, 0)$ as the unit-sample response $h[0, L-1]$ extended with $N - L$ zeros, (4.3) can be written as

$$\tilde{r}[0, N-1] = s[0, N-1] \circledast \tilde{h}[0, N-1] + n[0, N-1] \tag{4.4}$$

where $\circledast$ denotes the circular convolution operator. For this new channel model, The input constraint is

$$E[x_k^2] \leq E_s, \quad 0 \leq k < N \tag{4.5}$$

where E_s is the maximum per symbol average energy. The channel model described by (4.3) and (4.5) is called the N-circular Gaussian channel (NCGC). The capacity of the NCGC (in bits per channel input symbol when logarithms of base 2 is used) can be derived as follows [14]:

$$\tilde{C}_N(E_s) = (2N)^{-1} \sum_{i=0}^{N-1} \log[\max(\Omega |\tilde{H}_i|^2, 1)] \tag{4.6}$$

where $\tilde{H}[0, N-1]$ is the DFT of $\tilde{h}[0, N-1]$,

$$\tilde{H}_i = \sum_{m=0}^{N-1} \tilde{h}_m e^{-j2\pi m/N}, \quad 0 \leq i < N \tag{4.7}$$

and the parameter Ω is the solution of

$$\sum_{i=0,\tilde{H}_i\neq 0}^{N-1} \max(\Omega - |\tilde{H}_i|^{-2}, 0) = 2NE_s/N_0 \tag{4.8}$$

The method to obtain the value of the parameter Ω is as follows. By (4.8), the range of the Ω is bounded by $2NE_s/N_0 + \tilde{H}_{\min}^{-1}$ and $\tilde{H}_{\max}^{-1}$, where $\tilde{H}_{\max} = \max_i |\tilde{H}_i|^2$ and $\tilde{H}_{\min} = \min_i |\tilde{H}_i|^2$. The lower bound $\tilde{H}_{\max}^{-1}$ for Ω is from the fact that Ω should be greater than $\tilde{H}_{\max}^{-1}$. Otherwise, the summation in (4.8) sum up to zero. The upper bound $2NE_s/N_0 + \tilde{H}_{\min}^{-1}$ is from the observation that if Ω is greater than this value, then the summation exceed the right-hand-side value $2NE_s/N_0$. At the first step, this range is divided into 100 segments and the boundary values for each segment, denoted as $\Omega_i, i = 0, 1, \ldots, 100$, is tested by (4.8). For some k, Ω_k satisfies the inequality $\sum_{i=0,\tilde{H}_i\neq 0}^{N-1} \max(\Omega_k - |\tilde{H}_i|^{-2}, 0) - 2NE_s/N_0 \leq 0$ and Ω_{k+1} changes the sign of the inequality to $\sum_{i=0,\tilde{H}_i\neq 0}^{N-1} \max(\Omega_{k+1} - |\tilde{H}_i|^{-2}, 0) - 2NE_s/N_0 \geq 0$. If $\Omega_{k+1} - \Omega_k$ is smaller than a pre-determined threshold, then the procedure is stopped and Ω_k is the approximation value for Ω. Otherwise, set Ω_k and Ω_{k+1} as the lower and upper bound of the new range and divide it into 100 segments again and continue the same process.

Using the approximated Ω, which is accurate to the pre-determine threshold, and (4.6), I calculated the channel capacity with the channel impulse response measured at the girders under the bridge. The channel capacity at the first girder under the bridge is plotted in Figure 4.5. In Figure 4.5, I also provided the channel capacity without the knowledge of the channel information at the transmitter. The formula for the channel capacity in this scenario is as follows:

$$C(\gamma) = E[\log(1 + \gamma|\tilde{H}|^2)] \tag{4.9}$$

where γ is the ratio of average signal-to-noise power. To be specific, if we define
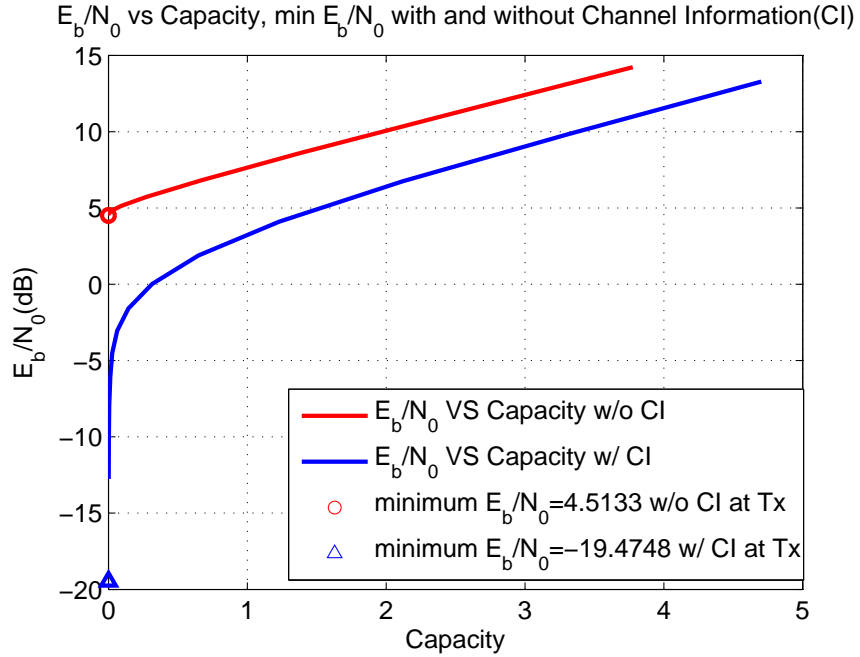
Figure 4.5: Channel capacity vs. $\frac{E_b}{N_0}$ and minimum $\frac{E_b}{N_0}$ at the 1st girder
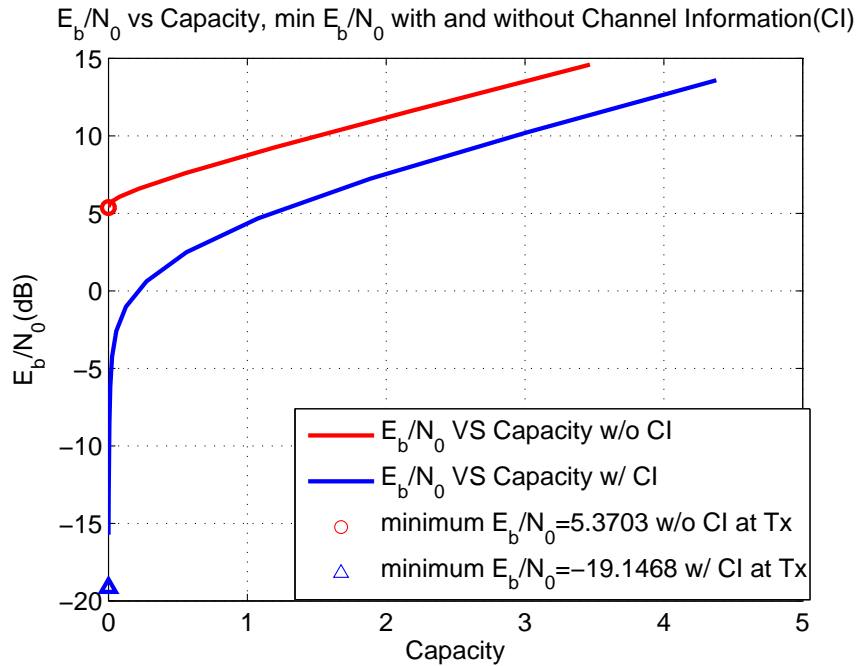
Figure 4.6: Channel capacity vs. $\frac{E_b}{N_0}$ and minimum $\frac{E_b}{N_0}$ at the 4th girder
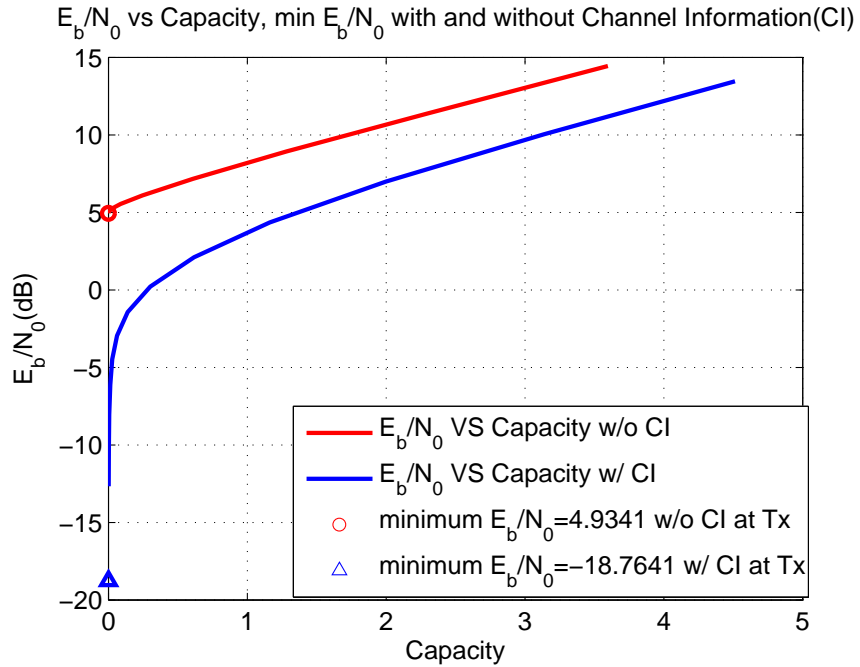
Figure 4.7: Channel capacity vs. $\frac{E_b}{N_0}$ and minimum $\frac{E_b}{N_0}$ at the 7th girder
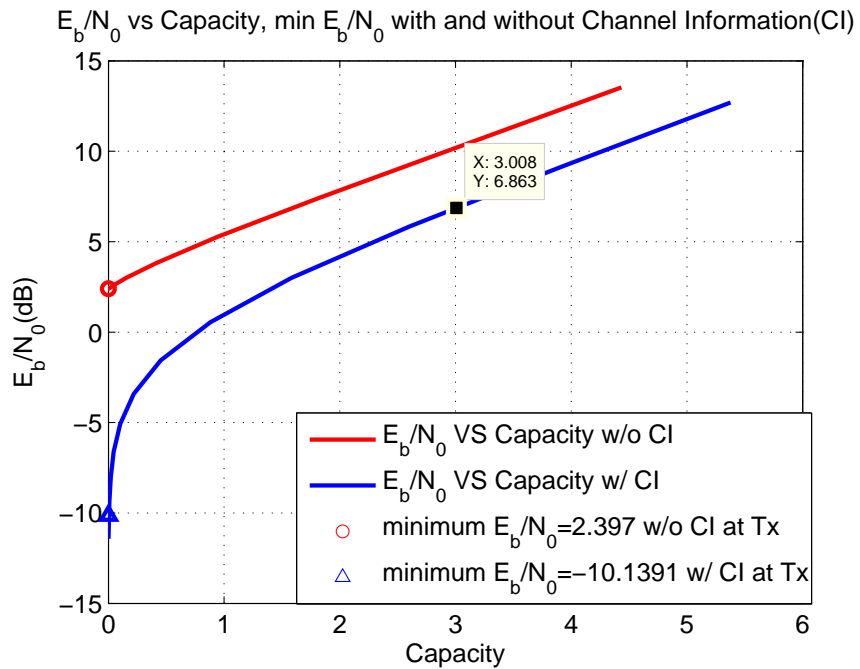
Figure 4.8: Channel capacity vs. $\frac{E_b}{N_0}$ and minimum $\frac{E_b}{N_0}$ across the bridge

$E[n_k^2] = \sigma^2$ and $E[x_k^2] \leq E_s$ for $0 \leq k < N$, then $\gamma = E_s/\sigma^2$. Moreover, the minimum $\frac{E_b}{N_0}$ without the channel information at the transmitter is derived by the following equation [30]:

$$\left(\frac{E_b}{N_0}\right)_{\min} = \frac{\ln 2}{E|\tilde{H}|^2]} \tag{4.10}$$

The minimum $\frac{E_b}{N_0}$ with the frequency-domain fading coefficients known at the transmitter is given as follows [30]:

$$\left(\frac{E_b}{N_0}\right)_{\min} = \frac{\ln 2}{\tilde{H}_{\max}} \tag{4.11}$$

The channel capacity with the channel impulse response measured at the 4th, the 7th girder, and across the bridge is presented in Figure 4.6, 4.7, and 4.8.

In these figures, I would like to point out the 4 to 5 dB gap in $\frac{E_b}{N_0}$ between the scenarios with the channel information and that without the channel information when capacity is larger than 1 bit per channel input symbol.

4.4   Conclusion

The channel model between sensors in UWB system under a bridge is not explicitly described in IEEE standard 802.15.4a. In this chapter, the channel measurement is performed under the bridge across Telegraph Road and the corresponding channel capacity is calculated. The obtained channel capacity provides the fundamental transmission rate limit in this specific environment. In comparison, the channel capacity in the case that the transmitter has no channel information is also presented in the figures. It is shown that the 5 dB gap $\frac{E_b}{N_0}$ between the transmitter with the channel information and that without the channel information. This result also can justify and motivate the channel estimation at receivers and provide feedback information to transmitters.

CHAPTER V

Signal Detection and Synchronization

5.1 Introduction

In Chapter III, it is assumed that the receivers have knowledge of system timing. This assumption is not practical in the real scenario and need to be addressed. if a receiver has no information about the time when the transmitter begins send a signal, the receiver cannot determine the proper starting time to perform the correaltion between the received signal and estimated channel template which is obtained by the method described in Chapter III. Several papers proposed methods to synchronize the UWB received signals with the corresponding transmitted signals. Carbonelli et.al [8] [7] used least square (LS) method to solve the signal synchronization problem in UWB system and also estimate the multipath channel impulse response but the proposed method requires a sampling rate of the same order as the inverse of a pulse duration. Rabbachin and Oppermann [28] apply energy collection on the received signal to reduced the sampling rate but their algorithm cannot perform the channel estimation at the same time. In this chapter, a method that can determine the timing of the received signal and also estimate the multipath channel is proposed.

Beyond solving the synchronization problem, a more fundamental issue is how one can determine whether the signal of interest is present at the receiver or not. Duarte et. al [13] presented a method to extract the largest component in the received

signal with matching pursuit and then compared the amplitude with a threshold. However, the threshold, which is found using Monte Carlo simulation, would depend on signal-to-noise ratio. Liu et. al [18] exploit the location information of the signal to solve the detection problem. They collected a certain number of the strongest components in the received signal and compared with a estimated template to count the number of strong components overlapping at the same location. Then, deciding the signal of interest is present when the number of overlapping components is over certain threshold. Nevertheless, the threshold is also dependent on SNR, which is usually hard to determine beforehand. The algorithm proposed here takes advantage of the autocorrelation characteristic of a repeated signal such that the threshold is independent of SNR. The approximated false alarm rate is also derived and provides guidance in choosing the integer threshold.

5.2 Signal Synchronization using Compressed Sensing

5.2.1 System Model

The system model assumed for the purposes of evaluating synchronization is the same model as in Section 3.1. The system uses ultra-short pulses $p(t)$. When sending N_f pulses $p(t)$, the kth binary information bit is transmitted with bit duration T_b. The frame duration $T_f = T_b/N_f$ is the time interval between the starting times of two consecutive pulses, $b(k) \in \{-1, 1\}$ is the binary information bit that is transmitted in the interval $[kT_b, (k+1)T_b]$ and modulates the amplitude of the pulses, and $p(t)$ is the pulse with duration $T_p \ll T_f$. Therefore, N_f nonoverlapped pulses are transmitted for each T_b. The transmitted signal can be written as

$$s(t) = \sum_k b(k) \sum_{j=0}^{N_f-1} p(t - jT_f - kT_b). \tag{5.1}$$

55

$$b(k) = 1, b(k+1) = \text{-}1, N_f = 5, T_b = N_f T_f$$
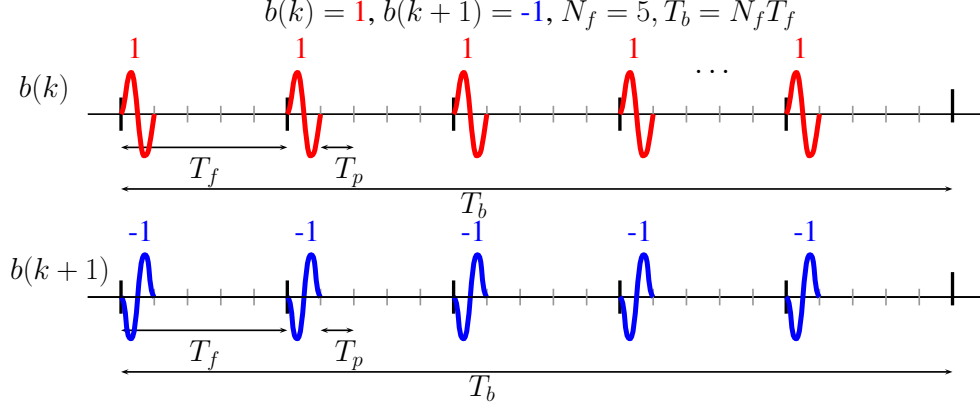
Figure 5.1: Transmitted signals

The same multipath channel model as in (3.3) is assumed with the following impulse response:

$$h(t) = \sum_{\ell=0}^{L-1} \alpha_\ell \delta(t - \tau_\ell). \tag{5.2}$$

where $\delta(\cdot)$ is the dirac delta function, τ_ℓ and α_ℓ are the delay and the gain associated with the ℓ-th propagation path of the UWB channel and L is the number of propagation paths. The channel is assumed to be static within N_s bits. Denote by $w(t)$ a zero-mean AWGN process and t_0 as the time offset between the transmitter and the receiver, which is assumed to be $0 \le t_0 < T_b$. The received signal can be described as:

$$r(t) = \sum_{k} b(k) \sum_{i=0}^{N_f-1} \sum_{\ell=1}^{L} \alpha_\ell p(t - jT_f - kT_b - t_0 - \tau_\ell) + w(t). \tag{5.3}$$

The received signal correpsonding to the k-th transmitted bit can be expressed as:

$$r_k(t) = b(k) \sum_{j=0}^{N_f-1} \sum_{\ell=1}^{L} \alpha_\ell p(t - jT_f - t_0 - \tau_\ell) + w(t). \tag{5.4}$$

56

The received signal corresponding to only the jth frame of the transmitted signal can be written as

$$r_f^j(t) = b(\lfloor \frac{j}{N_f} \rfloor) \sum_{\ell=1}^{L} \alpha_\ell p(t - jT_f - t_0 - \tau_\ell) + w(t) \tag{5.5}$$

$$= b(\lfloor \frac{j}{N_f} \rfloor) g(t - jT_f - t_0) + w(t) \tag{5.6}$$

where $g(t) = s(t) * h(t)$.

5.2.2   Optimal Receiver

In this subsection, the optimal receiver in the sense of maximum a posteriori (MAP) is analyzed. In order to simplify the derivation of the optimal receiver, the system model described in the previous subsection is transformed to discrete time domain. First, denote $t_0 = n_0 \Delta t$, where n_0 is an integer and Δt is a sampling parameter for sampling the continuous time signals $r_k(t)$, $g(t)$, and $r_f^j(t)$, and changing them to the discrete time signal $r_k[n] = r_k(n\Delta t)$ and $g[n] = g(n\Delta t)$ for $n = (k - 1)N_b, (k - 1)N_b + 1, \ldots, kN_b - 1$ and $r_f^j[n] = r_f^j(n\Delta t)$ for $n = (j - 1)N, (j - 1)N + 1, \ldots, jN - 1$, where $N_b = T_b/\Delta t$ and $N = T_f/\Delta t$. With the assumption that the synchronization offset n_0 takes the value in the range from 0 to N_b, equally likely, the MAP receiver becomes a maximum likelihood (ML) receiver. To derived the optimal receiver from the ML function, denote f as a probability density function for jointly Gaussian random vector $\mathbf{r}_k$. The ML detector can be described as maximizing conditional jointly Gaussian probability density function by varying n_0 and $\mathbf{g}$ as

follows:

$$\max_{n_0, \mathbf{g}} f(\mathbf{r}_k | n_0, \mathbf{g}) \tag{5.7}$$

$$= \min_{n_0, \mathbf{g}} \sum_{j=0}^{N_f-1} \sum_{n=0}^{N_b-1} (r_k[n + jN_b + n_0] - g[n])^2 \tag{5.8}$$

$$= \min_{n_0, \mathbf{g}} \sum_{j=0}^{N_f-1} \sum_{n=0}^{N_b-1} (r_f^j[n + n_0] - g[n])^2 \tag{5.9}$$

where N_b is the number of samples in one bit. The jointly minimization of the equation (5.9) is performed by seeking the values of $\mathbf{g}$ and n_0 as follows. In (5.9), taking the partial derivative with respect to $\mathbf{g}$, setting the result to zero, and solving for $\mathbf{g}$. Then $\tilde{\mathbf{g}}$ that minimizes (5.9) can be written as:

$$\tilde{g}[n] = \frac{1}{N_f} \sum_{j=0}^{N_f-1} r_f^j[n + \tilde{n}_0], \quad 0 \leq n \leq N_b - 1 \tag{5.10}$$

Next, substituting (5.10) into (5.9) to minimize (5.9) with respect to $\tilde{n}_0$ yields the following minimization:

$$\hat{n}_0 = \arg \min_{0 \leq \tilde{n}_0 \leq N_b-1} \sum_{j=0}^{N_f-1} \sum_{n=0}^{N_b-1} \left(r_f^j[n + \tilde{n}_0] - \frac{1}{N_f} \sum_{i=0}^{N_f-1} r_f^j[n + \tilde{n}_0] \right)^2. \tag{5.11}$$

Next, derive similar minimization equation as (5.11) using compressed sensing (CS). Let Φ be a $K \times N$ projection matrix. Define $g_{n_0}[n] = g[n - n_0]$ and $x_{n_0}[n] = x[n - n_0]$. Let $\mathbf{y}_f^j = \Phi \mathbf{r}_f^j$, where $\mathbf{y}_f^j = [y_f^j[0] \ y_f^j[1] \ \cdots \ y_f^j[N - 1]]^T$ and $\mathbf{r}_f^j = [r_f^j[0] \ r_f^j[1] \ \cdots \ r_f^j[N - 1]]^T$. Note that the projection matrix Φ is operated on the vector with the frame length N instead of the bit length N_b. Then, it can be written as

$$\mathbf{y}_f^j = \Phi \mathbf{r}_f^j = \Phi \mathbf{g}_{n_0} + \Phi \mathbf{w} = \mathbf{x}_{n_0} + \mathbf{u} \tag{5.12}$$

Define $\mathbf{y}_b = [(\mathbf{y}_f^1)^T \cdots (\mathbf{y}_f^{N_f})^T]^T$. The ML detector in CS case can be expressed in the

following equation:

$$\max_{n_0,\mathbf{x}} f(\mathbf{y}_b|n_0,\mathbf{x}) = \max_{n_0,\mathbf{x}} \sum_{j=0}^{N_f-1} \sum_{n=0}^{K-1} (y_f^i[n+n_0] - x[n])^2 \qquad (5.13)$$

Similarly, the minimization is performed on $\mathbf{x}$ and n_0 iteratively. With $\tilde{n}_0$ fixed, the $\mathbf{x}$ that maximize (5.13) can be derived by taking partial derivative with respect to $\mathbf{x}$ as follows:

$$\tilde{x}[n] = \frac{1}{N_f} \sum_{j=0}^{N_f-1} y_f^j[n+\tilde{n}_0], \qquad 0 \le n \le K-1 \qquad (5.14)$$

Substituting (5.14) into (5.13) and minimizing with respect to $\tilde{n}_0$, yields

$$\hat{n}_0 = \arg \max_{0 \le \tilde{n}_0 \le N-1} \left\{ \sum_{j=1}^{N_f-1} \sum_{n=0}^{K-1} \left[y_f^j[n+\tilde{n}_0] - \frac{1}{N_f} \sum_{i=0}^{N_f-1} y_f^i[n+\tilde{n}_0] \right]^2 \right\} \qquad (5.15)$$

5.2.3 Proposed Synchronization Method

In the previous subsection, the optimal receiver is introduced but the complexity is very high. In this subsection, a practical solution to synchronization problem is proposed. As a first step, the transmitter sends out $N_p N_f$ "+1" pulses to estimate
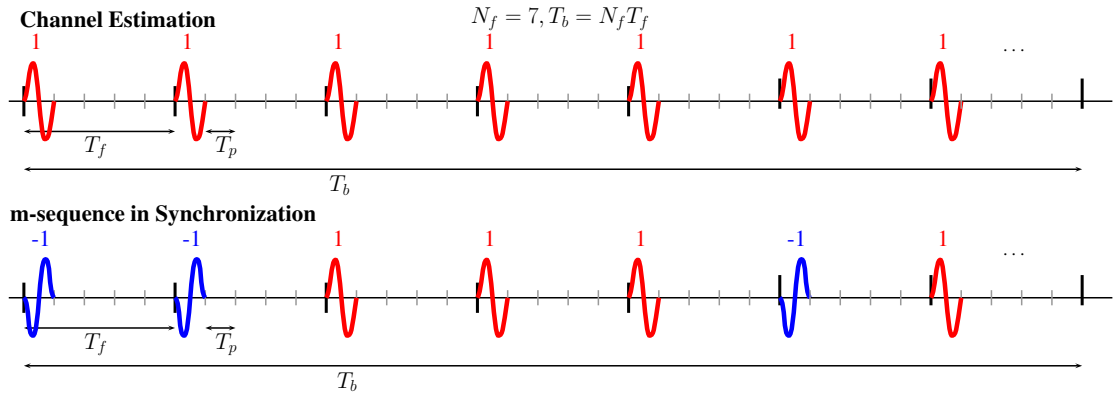

Figure 5.2: Transmitted signals

the multipath channel with time uncertainty up to one bit duration $T_b = N_f T_f$. This method to estimate the channel is resulted from (5.10) and the number of frames

Frame Offset	Codewords	Modulation Sequence
0	0011101	-1 -1 1 1 1 -1 1
1	1001110	1 -1 -1 1 1 1 -1
2	0100111	-1 1 -1 -1 1 1 1
3	1010011	1 -1 1 -1 -1 1 1
4	1101001	1 1 -1 1 -1 -1 1
5	1110100	1 1 1 -1 1 -1 -1
6	0111010	-1 1 1 1 -1 1 -1

Table 5.1: M-sequence codewords and modulation sequences

collected is increased from N_f to $N_p N_f$. Basically, the received signal is averaged over $N_p N_f$ frames, that is $\frac{1}{N_p} \frac{1}{N_f} \sum_{i=1}^{N_p} \sum_{j=0}^{N_f-1} r_f^j[n + iN_b + \tilde{n}_0]$ for $0 \le n \le N_b N_p - 1$, and MP algorithm is used to estimate the multipath channel as shown in the upper part of Figure 5.5 and 5.4. After estimating the channel, the transmitter starts to use a maximum length sequence (MLS, so-called m-sequence) to modulate pulses in each frame. For example, consider a m-sequence with codeword length 7 as shown in Table 5.1. The first line is chosen to modulate the signal and thus the pulses in each frame in one bit are modulated by the sequence "-1 -1 1 1 1 -1 1". Figure 5.2 shows the transmitted "+1" pulses to estimate the channel in the upper part and the transmitted pulses modulated by the m-sequence "-1 -1 1 1 1 -1 1" in the lower part. Note that codeword length must be chosen to be equal to the number of frames N_f. Since a MLS is one type of pseudorandom binary sequence, the advantage of MLS is that it has an autocorrelation function that has the largest value, $N_f(=7)$, when the time shift equals zero and the low value, -1, at the other time shift as shown in Figure 5.3. This advantage is exploited to determine the number of frame offsets between the transmitter and the receiver as described below. In the case of the correlator-base receiver, the each frame of received signal $r(t)$ is first correlated with the estimated channel template $g_{cs}(t)$ as shown in the lower part of Figure 5.4 and can be expressed

Figure 5.3: Autocorrelation function of modulation sequence

as:

$$z_k[j] = \int\limits_{jT_f+kT_b}^{(j+1)T_f+kT_b} r(t)g_{cs}(t - jT_f - kT_b)dt, \qquad (5.16)$$

where $z_k[j]$ is the corrrelated output of the jth frame in the kth bit. Denote m_i for $i = 0, 1, \ldots, N_f - 1$ as a i circular shifted vector of the modulation sequence "-1 -1 1 1 1 -1 1". For example, if N_f=7, $m_0 = [-1, -1, +1, +1, +1, -1, +1]$. Then the correlator output of the N_f(=7) frames in one bit and N_f(=7) different modulation sequences are calculated with inner product. Among N_f inner products, the largest one is pointed to the estimated number of frame offsets $\hat{f}_o$ between the transmitter and the receiver as follows:

$$\hat{f}_o = \arg\max_{i=0,1,\ldots,N_f-1} \sum_{j=kN_f+1}^{(k+1)N_f} z_k[j]m_i[j]. \qquad (5.17)$$

For example, if the largest inner product results from the 3rd line of the modulation sequence listed in Table 5.1, the frame offset is determined to be 2. Figure 5.4 shows the CS correlator receiver structure that can be adopted to estimate frame offsets

61

as described above.   Similarly, in the case of the rake receiver, the each frame of
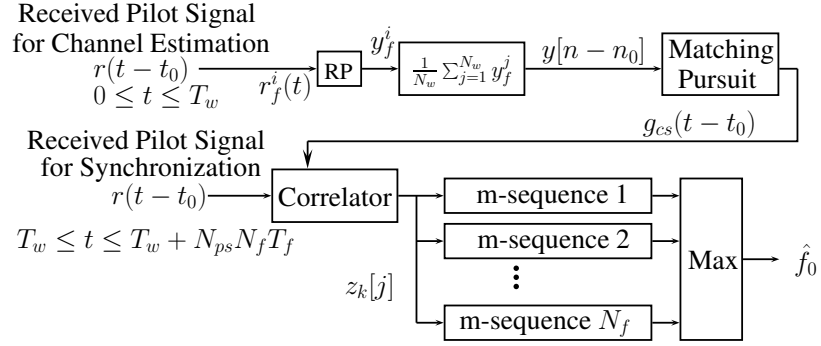
Figure 5.4: CS correlator receiver with frame offset estimation

Figure 5.5: CS rake receiver with frame offset estimation

received signal is first correlated with the L_c largest components in the estimated channel template as shown in the lower part of Figure 5.5 and can be expressed by:

$$z_R[k,j] = \sum_{\ell=1}^{L_c} \hat{\alpha}_\ell \int_{kT_b+jT_f+\hat{\tau}_\ell}^{kT_b+jT_f+\hat{\tau}_\ell+T_p} r(t)p(t - kT_b - jT_f - \hat{\tau}_\ell)dt, \qquad (5.18)$$

where $z_R[k,j]$ is the output sum of L_c correlators for the jth frame in the kth bit. The inner product of $z_R[k,j]$ and m_i for $i = 0, 1, \ldots, N_f - 1$ is calculated and the argument

i that maximizes the inner product is the estimated frame offset $\hat{f}_o$ as follows:

$$\hat{f}_o = \underset{i=0,1,...,N_f-1}{\arg\max} \sum_{j=kN_f+1}^{(k+1)N_f} z_R[k,j]m_i[j]. \tag{5.19}$$

Figure 5.5 shows the CS rake receiver structure used to estimate frame offset as described above.

The result of frame synchronization error rate (SER) v.s. E_b/N_0 is shown in Figure 5.6, where N_{ps} is the number of pilot bits used to estimate the frame offset and N_p is the number of pilot bits used to estimate the multipath channel. To calculate SER, the actual time offset n_0 is recorded, divided by the number of samples in one frame N, and take the floor operation to obtain the integer value of frame offset $\lfloor \frac{n_0}{N} \rfloor = f_o$. Then, the estimation of frame offset $\hat{f}_o$ using a m-sequence is compared with f_o. If $\hat{f}_o \neq f_o$, one error occurs and the total error is divided by number of testing bits to obtain SER. It is observed that the SER approaches flat starting with E_b/N_0 around
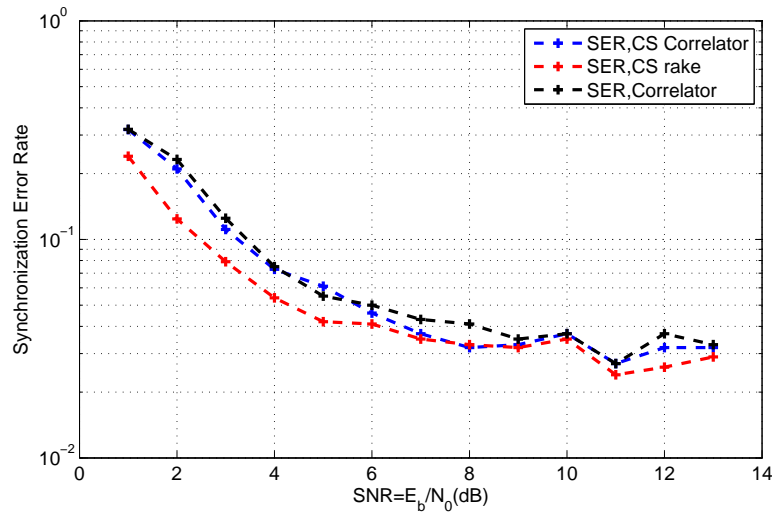

Figure 5.6: Frame synchronization error rate, K=720, N_p=128, N_f=7, N_{ps}=10

6 to 8 (dB). This can be explained by the reason that the multipath components may span cross different frames, say the 2nd and the 3rd frame for instance. With
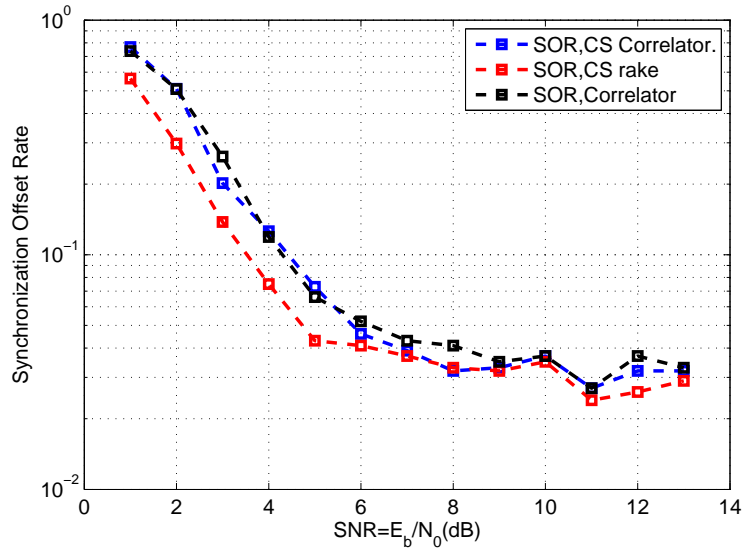
Figure 5.7: Frame synchronization offset rate, K=720, N_p=128, N_f=7, N_{ps}=10

certain probability, the more signal energy could be split into the 3rd frame. When this occurs, it is more likely that the inner product resulting from the 3rd modulation sequence is higher than that from the 2nd modulation sequence. The estimated number of the frame offset $\hat{f}_o$ is determined as 3 while f_o=2 so an estimation error on frame timing occurs.

Figure 5.7 shows synchronization offset rate (SOR) v.s E_b/N_0, where SOR is defined as the number of frame offsets per bit. The SOR is calculated by summing up $|f_o - \hat{f}_o|$ and then dividing by total number of testing bits. In Figure 5.7, the SOR also becomes flat when the SNR reaches around 6 to 8 (dB). The same reason described above can be applied to explain this phenomenon.

The frame offset mean square error (FMSE), which is defined as the average of $(\frac{n_0}{N} - \hat{f}_o)^2$ per bit, is also shown in Figure 5.8. It illustrated that FMSE also becomes flat when SNR reaches 6 to 8 (dB).

The BER performance for perfect synchronized and unsynchronized receiver used proposed synchronization algorithm is shown in Figure 5.9. Notice that the BER maintain waterfall curve even when SNR reaches 8 (dB) and beyond and the perfor-
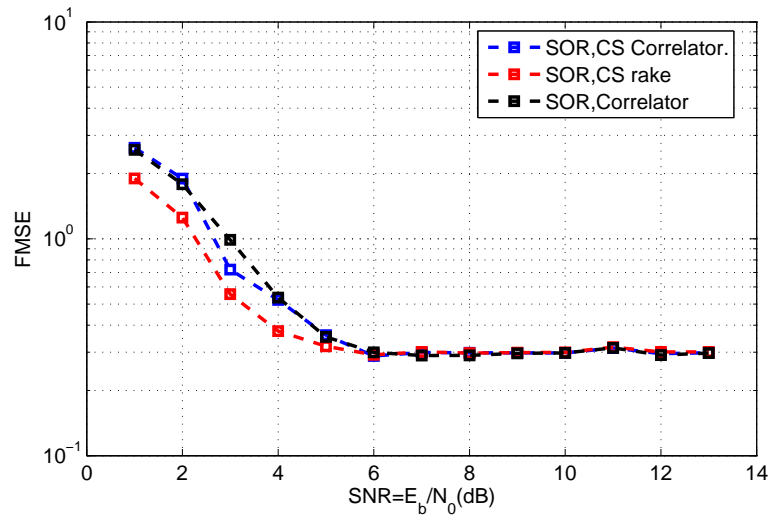
Figure 5.8: Frame synchronization offset mean square error rate, K=720, N_p=128, N_f=7, N_{ps}=10
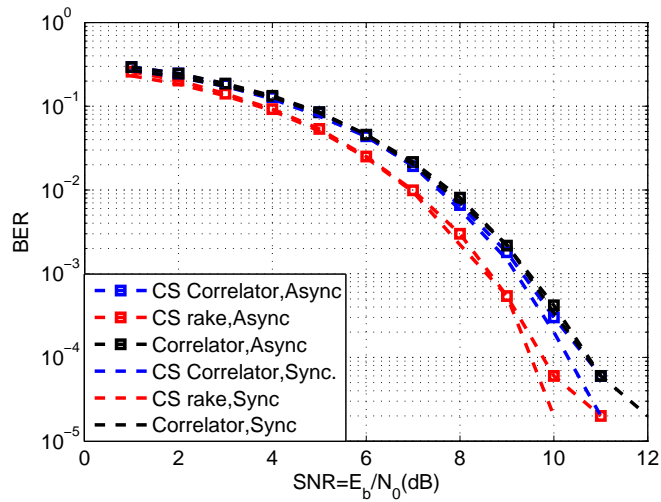

Figure 5.9: Bit error rate, K=720, N_p=128, N_f=7, N_{ps}=10

65

mance is very close to the one with perfect synchronization. This shows that receiver can detect the information bit and is robust even though the certain amount of the frame offset occurs.

5.3 Detection of Signal Presence

In previous section, the method of signal synchronization using compressed sensing is introduced. A more fundamental problem is how one determine whether a signal is transmitted or not. In this section, a method to detect signal presence is proposed to solve the problem. The advantage of this method is that the threshold to determine the existence of signal is independent of signal-to-noise ratio. The algorithm is described as follows.

5.3.1 Detection Model

This detection problem can be formed as a hypothesis testing problem. Define H_0 as the null hypothesis that no signal is transmitted and H_1 as a signal is transmitted. Considering the discrete time domain, let $\mathbf{r}$ be the received signal, $\mathbf{g} = \mathbf{s} * \mathbf{h}$, where $\mathbf{s}$ is the transmitted signal and $\mathbf{h}$ is the channel impulse response, and $\mathbf{w}$ is the additive white Gaussian noise (AWGN). The discrete time formulation can be expressed as:

$$H_0 \quad : \quad \mathbf{r} = \mathbf{w}, \tag{5.20}$$

$$H_1 \quad : \quad \mathbf{r} = \mathbf{g} + \mathbf{w}. \tag{5.21}$$

where $w \sim N(0, \sigma^2 I_N)$ be i.i.d. Gaussian noise. According to [10], given the the signal $\mathbf{g} \in \mathbb{R}^{N_b}$ is known, with the false alarm set to be $P_{FA} = \alpha$, the detection possibility is as follows:

$$P_D(\alpha) = Q\left(Q^{-1}(\alpha) - \sqrt{\frac{\mathbf{g}^T \mathbf{g}}{\sigma}}\right) \tag{5.22}$$

However, the threshold for this optimal result is dependent on SNR and $\mathbf{g}$ is known, where in practice these two terms is hard to obtain at receivers beforehand. On the contrary, the proposed method is independent of SNR as described below.

For each transmitted pilot bit $\mathbf{s}$, the Barker code with the length N_f is used, which is the same as the number of frame in one bit. For example, if $N_f=3$, the Barker code with length 3 is $[+1, +1, -1]$ and the transmitted signal $\mathbf{s} = [\mathbf{s}_1 \ \mathbf{s}_2 \ \mathbf{s}_3]^T$ can be pictured in Figure 5.10, where $\mathbf{s}_i$, for $i = 1, 2, \ldots, N_f$, is the ith frame in the transmitted signal $\mathbf{s}$. With the Barker code $[+1, +1, -1]$, the pulses in the first and second frames $\mathbf{s}_1$ and $\mathbf{s}_2$ are modulated by $+1$ and the pulse in the third frame $\mathbf{s}_3$ is modulated by -1. Next, considering that $\mathbf{s}$ is cyclic shifted by n_0 time samples (for
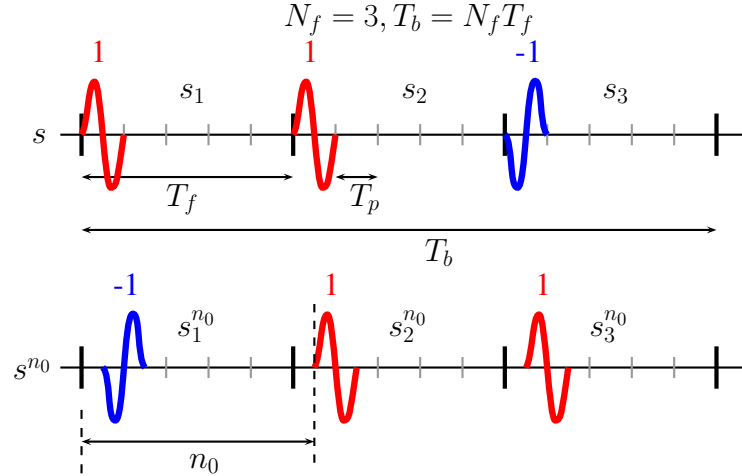
Figure 5.10: Transmitted signal s and shifted template $\mathbf{s}^{n_0}$

$n_0 = 0, 1, \ldots, N_b - 1$ and $N_b = NN_f$ is the number of samples in one bit) and the corresponding shifted signal is denoted by $\mathbf{s}^{n_0} = [\mathbf{s}_1^{n_0} \ \mathbf{s}_2^{n_0} \ \mathbf{s}_3^{n_0}]^T$ as shown in Figure 5.10. Then, $\mathbf{s}^{n_0}$ is the templates used to correlate with the received signals $\mathbf{r}$. With this notation, the proposed detection of signal presence is described as follows:

First, for the ith bit with N_f frames, the inner product of $\mathbf{s}^{n_0}$ and $\mathbf{r}$ is calculated

and the maximizer $\hat{k}_i$ for the ith bit is obtained in the following equation:

$$\hat{k}_i = \arg \max_{n_0} \langle \mathbf{s}^{n_0}, \mathbf{r} \rangle \tag{5.23}$$

This process is iterated for N_p bits and notice that for each iteration one may record different values of $\hat{k}_i$. Next, among N_p bits, the number of times $\hat{k}_i$ occurred for different values k, for $k = 0, 1, \ldots, N_b - 1$ is counted. In other words, since the maximizer of the ith bit is denoted as $\hat{k}_i$, the following determines the number of times that $\hat{k}_i = k$:

$$n_k = \sum_{i=1}^{N_p} I\{\hat{k}_i = k\} \tag{5.24}$$

where $I\{\cdot\}$ is the indicator function. Last, the $\max_k n_k$ is compared with an integer threshold to determine whether there is a signal transmitted or not. The threshold is chosen such that the criteria of the false alarm (FA) rate is satisfied. Figure 5.11 illustrate the concept of the proposed detection algorithm as describe above. In Figure 5.11, $s[n]$ is the transmitted signal, $g[n] = s^{n_0}[n] * h[n]$ is the received signal with timing offsets n_0 but without noise, $r[n] = g[n] + w[n]$ is the received signal with timing offsets and noise. If there is no noise in the received signal, the peaks of the correlation between $g[n]$ and $s^k[n]$ (k-shifted $s[n]$ for $k = 0, 1, \ldots, N_b - 1$) occurs at the same location $\hat{k}$ within every bit duration N_b. Hence, the number of times the peak occurring at the same location, that is, n_k is equal to N_p. As long as the threshold is chosen to be smaller than N_p, the receiver determines the signal is present. If noise is added into the received signal, the peak of correlation between $r[n]$ and $s^k[n]$ within each bit may occurs at the different locations. In this case, if the number of times the peaks occurs at any location n_k is not more than the threshold. The receiver declares no signal is transmitted only noise.

Consider the same hypothesis testing problem with compressed measurement, that
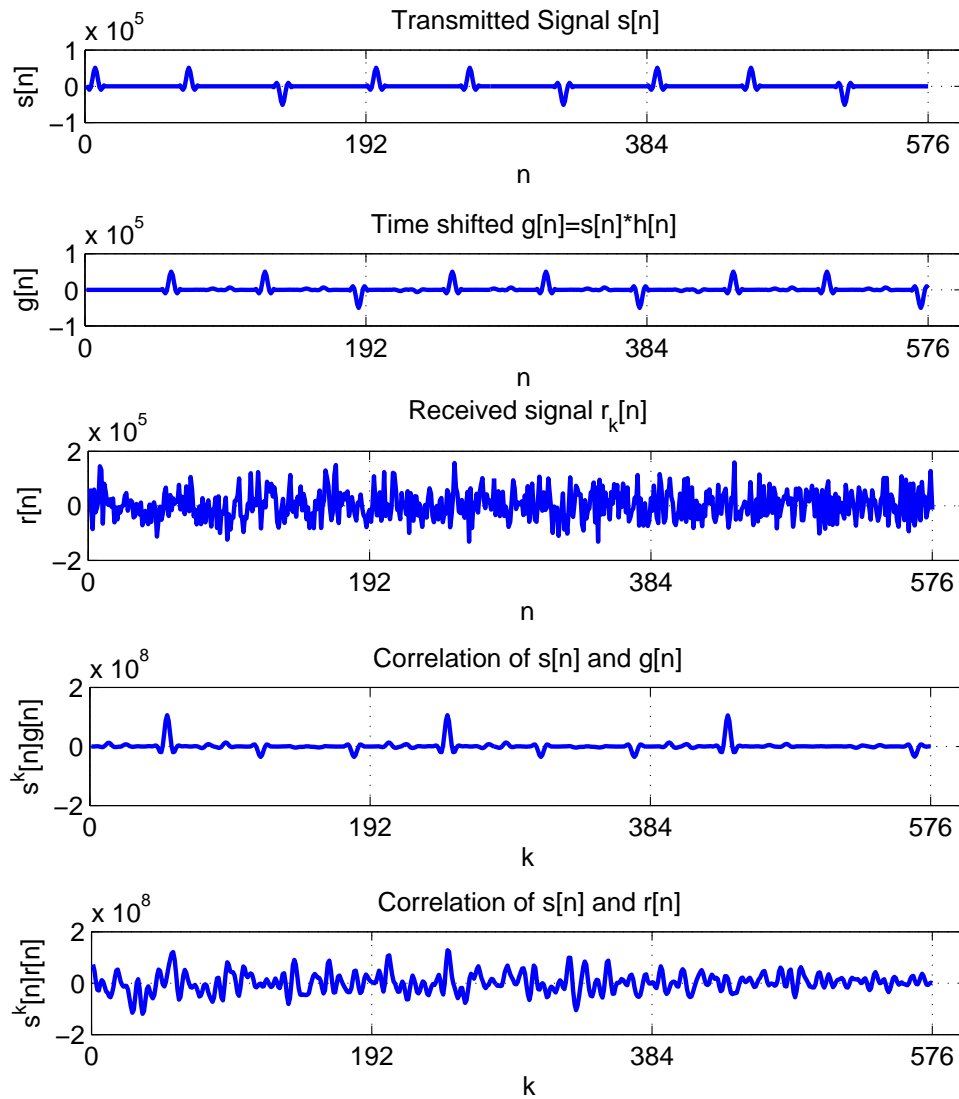
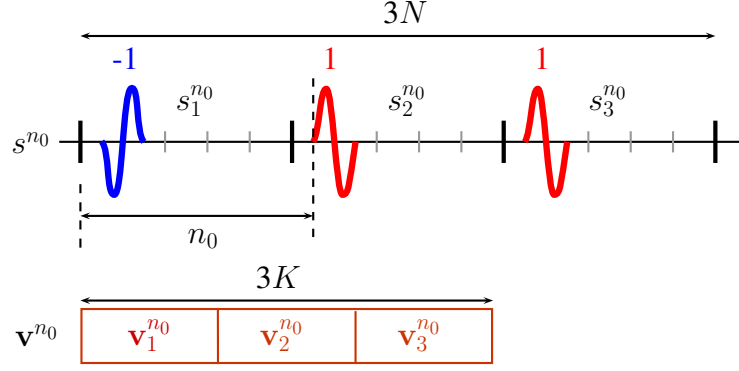Figure 5.11: Illustration of the detection concept, N_b=192

Figure 5.12: Shifted transmitted signal $\mathbf{s}^{n_0}$ and projected template $\mathbf{v}^{n_0} = \Phi \mathbf{s}_i^{n_0}$

is:

$$\tilde{\mathcal{H}}_0 : y = \Phi w \tag{5.25}$$

$$\tilde{\mathcal{H}}_1 : y = \Phi(g + w) \tag{5.26}$$

where $\Phi = [\phi_1 \ \phi_2 \cdots \ \phi_\mathbf{N}]$ is a $K \times N$ projection matrix and $w \sim \mathcal{N}(0, \sigma^2 I_N)$ is i.i.d. Gaussian noise. According to [10], given $\mathbf{g}$ is known at receivers and the false alarm probability $P_{FA} = \alpha$, the corresponding detection rate P_D can be expressed by:

$$P_D(\alpha) = Q\left(Q^{-1}(\alpha) - \frac{\sqrt{\mathbf{g}^T \Phi^T (\Phi\Phi^T)^{-1} \Phi \mathbf{g}}}{\sigma}\right) \tag{5.27}$$

This result is derived from the fact that the threshold for the detection is also dependent of SNR and the $\mathbf{g}$ is known at receivers, which is basically impractical for receivers to have this information in advance.

The threshold of the proposed detection algorithm described below is independent of SNR using compressed sensing. The projected vectors for each frame $\mathbf{s}_i^{n_0}$ in $\mathbf{s}^{n_0}$ is denoted by $\mathbf{v}_i^{n_0} = \Phi \mathbf{s}_i^{n_0}$, for $n_0 = 0, 1, \ldots, N_b - 1$ and shown in Figure 5.12. Define $\mathbf{y} = [\mathbf{y}_1 \ \mathbf{y}_2 \ \cdots \mathbf{y}_{N_f}]^T$ and $\mathbf{y}_i = \Phi \mathbf{r}_i$ for $i = 1, 2, \ldots, N_f$. Denote $\mathbf{v}^{n_0} = [\mathbf{v}_1^{n_0} \ \mathbf{v}_2^{n_0} \ \mathbf{v}_3^{n_0}]^T$ for $n_0 = 0, 1, \ldots, N_b - 1$ Then, $\mathbf{v}^{n_0}$ is the templates used to correlate with the pro-

jected received signals $\mathbf{y}$. The proposed detection of signal presence using compressed sensing is described as follows:

First, for the ith bit with N_f frames, compute the inner product of $\mathbf{v}^{n_0}$ and $\mathbf{y}$ for $n_0 = 0, 1, \ldots N_b - 1$ and record the $\hat{k}_i^c$ that maximizes the inner product for $i = 1, 2, \ldots, N_p$, that is,

$$\hat{k}_i^c = \arg \max_{n_0} \langle \mathbf{v}^{n_0}, \mathbf{y} \rangle \tag{5.28}$$

This process is performed over N_p bits and notice that for each bit one may record different values of $\hat{k}_i^c$. Next, among N_p bits, the number of times $\hat{k}_i^c$ occurred for different values k, for $k = 0, 1, \ldots, N_b - 1$ is counted. In other words, since the maximizer of the ith bit is denoted as $\hat{k}_i^c$, the following equation determines the number of times that $\hat{k}_i^c = k$:

$$n_k^c = \sum_{i=1}^{N_p} I\{\hat{k}_i^c = k\}. \tag{5.29}$$

Last, the $\max_k n_k^c$ is compared with an integer threshold to determine whether there is a signal transmitted or not. The threshold is chosen such that the criteria of the false alarm (FA) rate is satisfied. The approximation of the false alarm rate will be derived next.

5.3.2 False Alarm Rate Analysis

Consider the null hypothesis $H_0 : \mathbf{r} = \mathbf{w}$. The compressed measurement for $\mathbf{r}_i$, the ith frame of the received signal $\mathbf{r}$, can be written as:

$$\mathbf{y}_i = \Phi \mathbf{r}_i = \Phi \mathbf{w}_i \tag{5.30}$$

The inner products of $\mathbf{v}_i^{no}$ and $\mathbf{y}_i$ for $n_0 = 0, 1, \ldots, N_b - 1$ and $i = 1, 2, \ldots, N_f$ can be expressed as:

$$\langle \mathbf{v}_i^{no}, \mathbf{y}_i \rangle \tag{5.31}$$

$$= \langle \mathbf{v}_i^{no}, \phi_1 w_{i1} + \cdots + \phi_N w_{iN} \rangle \tag{5.32}$$

$$= \left(\sum_{j=1}^{K} \mathbf{v}_{ij}^{no} \phi_{1j} \right) w_{i1} + \cdots + \left(\sum_{j=1}^{K} \mathbf{v}_{ij}^{no} \phi_{Nj} \right) w_{iN} \tag{5.33}$$

Notice that the length of $\mathbf{v}_i^{no}$ is K so the summation is from 1 to K. To simplify the derivation for FA rate, one can assume that the terms $w_{i\ell}(\sum_{j=1}^{K} \mathbf{v}_{ij}^{no} \phi_{Nj})$ for $\ell = 1, 2, \ldots, N$ are mutually independent. The approximation of FA rate with this assumption is close to the actual FA rate without this assumption and will be shown in the simulation later. Using this assumption, the derivation of the FA rate for threshold=1 can be expressed in the following equation:

$$P_{FA} = 1 - P(\max_k n_k \leq 1 | H_0) \tag{5.34}$$

$$= 1 - \left(\frac{N_b - 1}{N_b} \right) \times \cdots \times \left(\frac{N_b - N_p + 1}{N_b} \right) \tag{5.35}$$

where $N_b = NN_f$. This is actually the same as the birthday problem that there are N_b days in one year and the probability P_{FA} is among N_p people more than one person have the same birthday. However, considering the case for threshold $=2$, one needs the solution to the generalized birthday problem [22] to solve the false alarm rate. With the definition of S_2 as the set such that for every $k \in S_2$, $n_k = 2$, where n_k is calculated by (5.24), and $|S_2|$ as the number of elements in S_2, one can write

the FA probability as follows:

$$P_{FA} = 1 - P(\max_k n_k \leq 2|H_0) \tag{5.36}$$

$$= 1 - \sum_{i=1}^{\lfloor N_p/2 \rfloor} P(|s_2| = i|H_0) - P(n_k \leq 1, \forall k|H_0) \tag{5.37}$$

$$= 1 - \sum_{i=1}^{\lfloor N_p/2 \rfloor} \frac{N_b!}{N_b^{N_p} i! (N_p - 2i)! (N_b + i - N_p)!} \frac{N_p!}{(2!)^i} - \frac{N_b!}{(N_b - N_p)! N_b^{N_p}} \tag{5.38}$$

Given the threshold $= 3$, similarly, define S_3 as the set such that for every $k \in S_3$, $n_k = 3$ and $|S_3|$ as the number of elements in S_3, and then the corresponding FA probability can be expressed as:

$$P_{FA} = 1 - P(\max_k n_k \leq 3|H_0) \tag{5.39}$$

$$= 1 - \sum_{\substack{i,j \geq 0 \\ 2i+3j \leq N_p}} P(|S_2| = i, |S_3| = j|H_0) \tag{5.40}$$

$$= 1 - \sum_{\substack{i,j \geq 0 \\ 2i+3j \leq N_p}} \frac{N_b!}{N_b^{N_p} i! j! (N_p - 2i - 3j)! (N_b - N_p + i + 2j)!} \frac{N_p!}{(2!)^i (3!)^j} \tag{5.41}$$

Define the following equation:

$$P(i, j) = P(|S_2| = i, |S_3| = j|H_0) \tag{5.42}$$

Then, notice that $P(0,0) = \frac{N_b!}{N_b^{N_p} (N_b - N_p)!} = P(n_k \leq 1, \forall k|H_0)$. Last, the derivation of the FA rate for threshold$=4$ can be expressed as follows:

$$P_{FA} = 1 - P(\max_k n_k \leq 4|H_0) \tag{5.43}$$

Define S_4 be the set such that for every $k \in S_4$, $n_k = 4$. Denote $|S_4|$ as the number of elements in S_4. Then, the probability $P(\max_k n_k \leq 4|H_0)$ can be calculated by the

following equation:

$$P(\max_k n_k \leq 4|H_0) = \sum_{\substack{i,j,k \geq 0 \\ 2i+3j+4k \leq N_p}} P(i,j,k), \tag{5.44}$$

where

$$P(i,j,k) = P(|S_2| = i, |S_3| = j, |S_4| = k|H_0) \tag{5.45}$$

$$= \frac{1}{N_p} \frac{N_b!}{i!j!k!(N_p - 2i - 3j - 4k)!(N_b - N_p + i + 2j + 3k)!} \frac{N_p!}{(2!)^i(3!)^j(4!)^k}. \tag{5.46}$$

5.3.3 Simulation Results

In this section, the simulated FA rate and the approximated FA rate is first illustrated with different N_p. Then, the detection rates with different thresholds and N_p are shown to demonstrate the performance of the proposed algorithm. In the simulation, the parameters of the system are set as follows: $N=64$, $K=48$, and $N_f=7$. The simulated false alarm rate and the approximation FA rate with the assumption that the terms $w_{i\ell}(\sum_{j=1}^{K} \mathbf{v}_{ij}^{n_0} \phi_{Nj})$ are mutually independent are shown in Figure 5.13. Recall that the received signal is first process by a $K \times N$ projection matrix Φ. One can observe that the two curves are close to each other, which means the assumption is valid. Figure 5.14 shows the FA rate versus different thresholds without projection matrix multiplying on the received signal. In this case, the assumption that inner product $\langle \mathbf{s}^{n_0}, \mathbf{w} \rangle$ for $n_0 = 0, 1, \ldots, N_b$ are mutually independent is also valid since the two curves are very close. Next, the number of pilots N_p is changed to 100. In this case, the FA rate increases as expected in the formula and shown in Figure 5.15 and Figure 5.16. In Figure 5.14 and 5.16, one can observe that the curves based one the approximation is lower than the curve based on simulation in the case where no projection matrix is applied to the received signal. This could be be due to the fact that in simulation scenario, the inner product terms $\langle \mathbf{s}^{n_0}, \mathbf{w} \rangle$ are slightly corre-
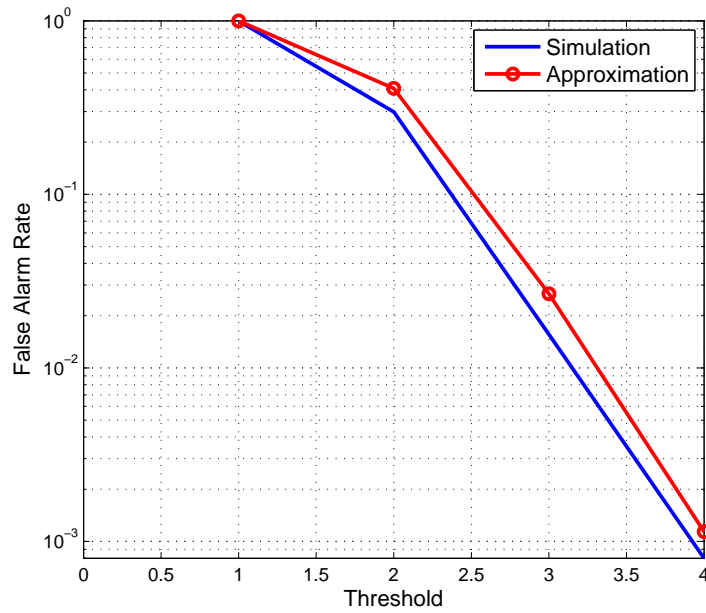
Figure 5.13: False alarm rate v.s threshold with received signals processed by projection matrix Φ, $K=48$, and $N_p=75$
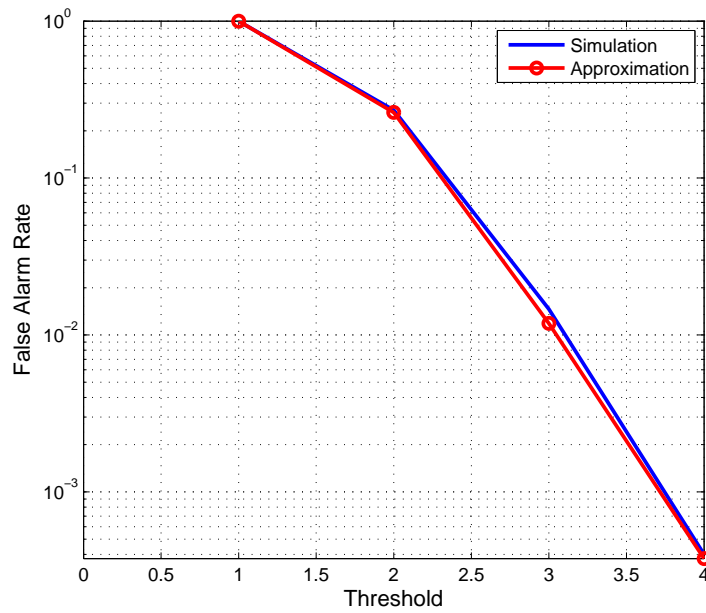

Figure 5.14: False alarm rate v.s threshold without received signals processed by projection matrix Φ, $N=64$, and $N_p=75$
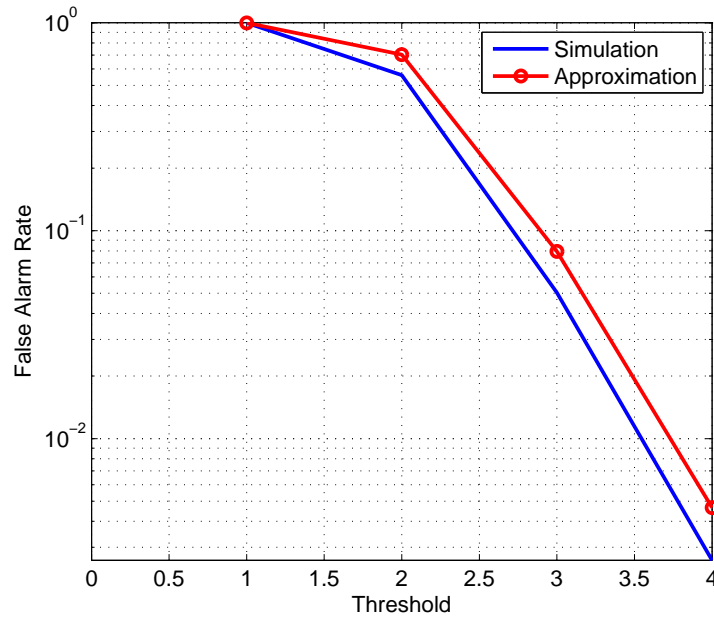
Figure 5.15: False alarm rate v.s threshold with received signals processed by projection matrix Φ, K=48, and N_p=100
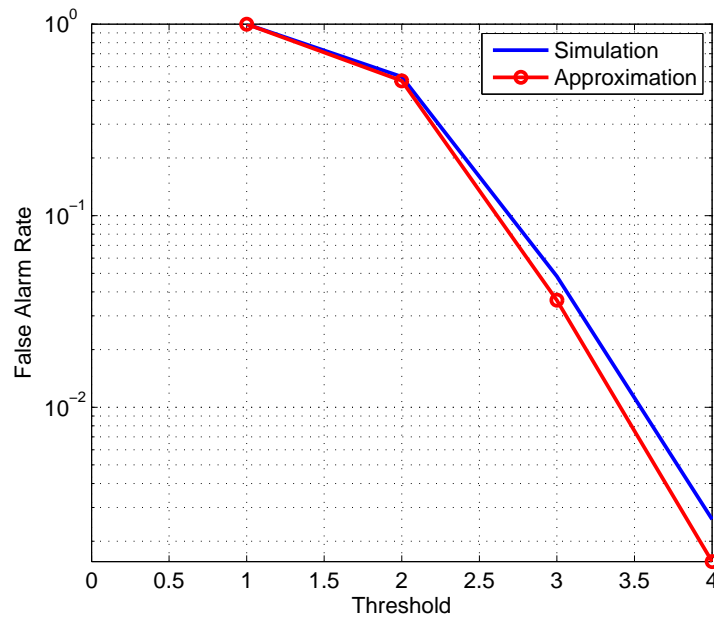

Figure 5.16: False alarm rate v.s threshold without received signals processed by projection matrix Φ, N=64, and N_p=100

lated so the probability $\max_k n_k$ greater than the threshold is likely larger. In Figure 5.13 and 5.15, the approximation curve is plotted with $K_b = KN_f$=336 instead of $N_b = NN_f$=448, and thus the FA rate calculated by approximation is higher than the FA rate by simulation. It is because in the simulation, the possible time shift n_0 is range from 0 to $N_b - 1$ even though the length of the vectors $\mathbf{v}^{n_0}$ is K_b. Hence, it is reasonable that the simulation curve falls below the approximation curve.
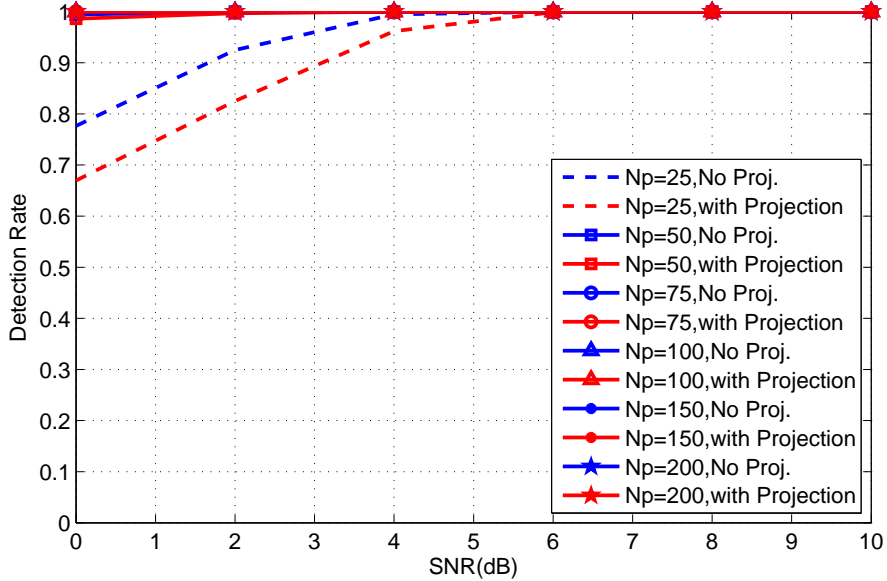

Figure 5.17: Detection rate v.s SNR, for threshold=1 and different N_p

Figure 5.17, 5.18, 5.19, and 5.20 show the detection rate for different number of pilot bits N_p from 25 to 200 and for different thresholds, respectively. One can observe that when received signals are processed by compressed measurement matrix Φ, the performance degrade at low SNR. However, choosing N_p large enough reduces the the performance loss at low SNR. These figures show that for N_p=75, the detection performance yield good results combined with the false alarm rate results shown before. Figure 5.19 also demonstrates the performance compared to optimal detection described in (5.22). It is observed that for N_p=25, the proposed algorithm requires extra 5 to 6 dB to achieve the same detection rate as the optimal detection. However,
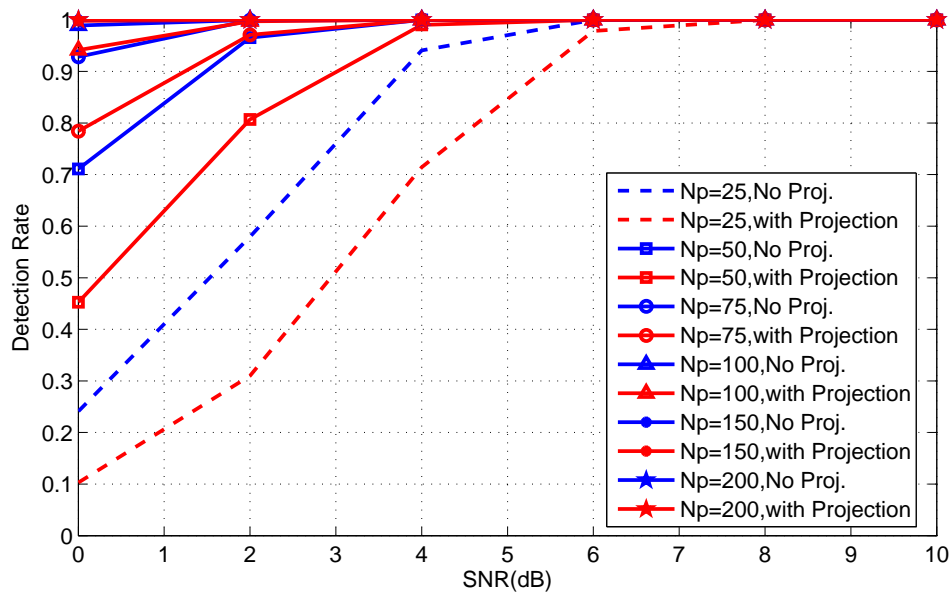
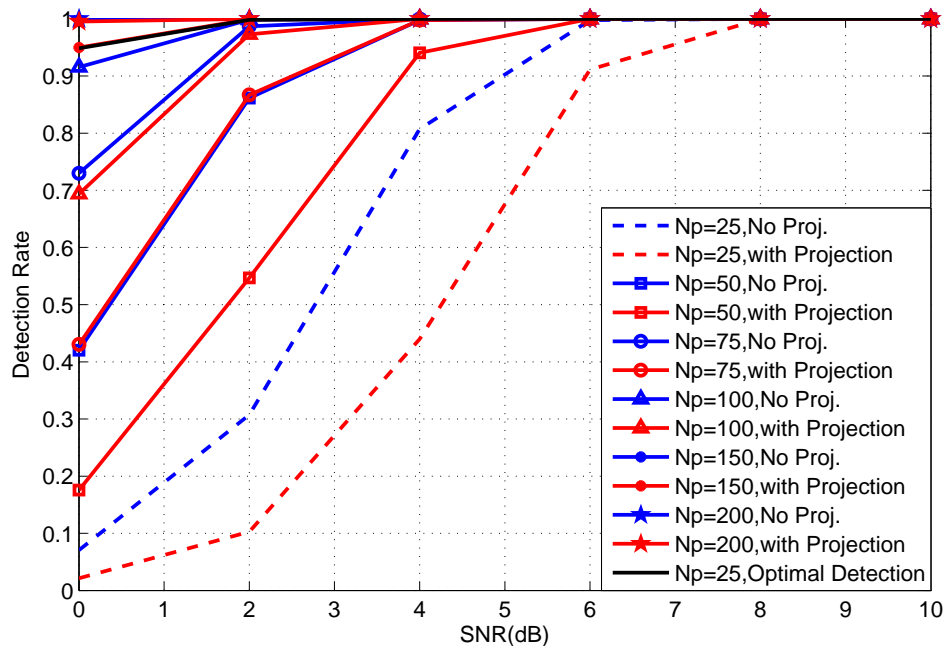Figure 5.18: Detection rate v.s SNR, for threshold=2 and different N_p

Figure 5.19: Detection rate v.s SNR, for threshold=3 and different N_p, compared with optimal detection
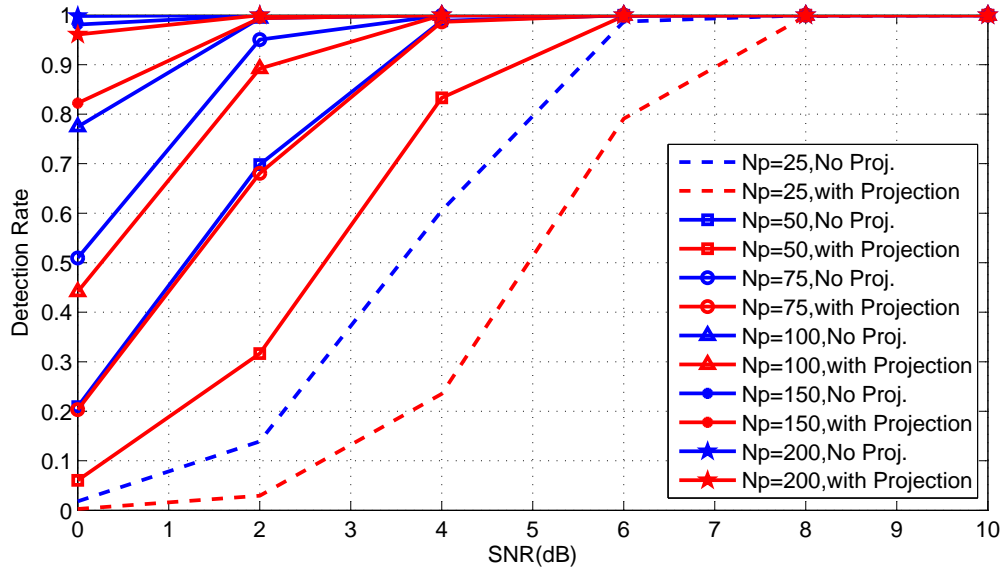
Figure 5.20: Detection rate v.s SNR, for threshold=4 and different N_p

the optimal detection is not practical since the knowledge of the signal **g** and SNR is needed at receivers in advance.

5.4 Conclusion

In this chapter, the algorithms to synchronize the signal and to detect the existence of signal are proposed. Using m-sequences and compressed sensing, the proposed synchronization algorithm can determine the frame offsets between the transmitted and received signal and estimate the channel estimation at the same time while the required sampling rate is on the order of inverse of a frame duration instead of a pulse duration. The BER performance of unsynchronized receivers using proposed synchronization algorithm is shown to be very close to that with perfect synchronized receivers.

Exploiting the Barker code and autocorrelation of repeated signals, one can determine the signal presence and the threshold is independent of SNR in my proposed algorithm. With the independence assumption of the received signal under the null

hypothesis, the approximated false alarm probability is also derived and shown to be close to the simulation result. When the threshold equals to 2 or 3, the system with N_p=75 provides a sufficient detection rate while maintaining a low false alarm rate.

CHAPTER VI

Conclusion

6.1 Conclusion

In this thesis, the method to use the compressed sensing with reduced sampling rate on received signals to reconstruct the multipath channel template is described. The different coding and projection schemes including using a Hadamard matrix are also introduced. Furthermore, the different receiver structures which reduce the complexity of implementation is presented. The BER performance of CS-correlator and CS-rake receivers is evaluated and compared with the conventional correlator by changing the parameters such as number of pilot bits N_p, number of projections K, and number of finger L_c in rake receivers. It can be observed that when these parameters increase, the BER performance improves. The possible choices for these parameters are also provided. The practical implementation scenario where the finite bits resolution is restricted on channel estimation is considered and the effect of finite bit resolution on BER performance is demonstrated.

Since IEEE 802.15.4a standard only provides channel models for indoor and outdoor but on specific for bridges, the channel measurement is performed under the bridge carrying I-275 across Telegraph Road, where the sensors are deployed in our project. The channel capacity based on the measurement of channel impulse response obtained at the different girders under the bridge across Telegraph Road is evaluated

with and without channel knowledge at transmitters.

It is important and practical to investigate the algorithm to detect the existence of signals and the synchronization of signals at receivers. Hence, the method of the detection and synchronization of signals in UWB system using compressed sensing technique is proposed. The m-sequence is used to estimate the frame offset and Barker code and autocorrelation of the repeated signals are exploited to determine the existence of the signal of interest. The BER performance of a unsynchronized receiver with proposed synchronization algorithm is very close to a receiver with perfection synchronization despite the fact that the synchronization error rate becomes flat at high SNR. This demonstrates that the propose synchronization algorithm is robust to detect the transmitted information bits even when some synchronization errors occurred. The proposed algorithm to detect the signal presence provides the threshold which is independent of SNR at receivers. The false alarm analysis is derived with the assumption that the inner product of projected received signal $\mathbf{y}$ ($=\mathbf{w}$ in H_0) and projected templates $\mathbf{v}$ are mutually independent. This assumption is illustrated to be a reasonable approximation by simulated figures. The simulation figures suggest that with the threshold equaling to 3, the $N_p=75$ provides promising detection rate while remaining low false alarm rate.

6.2 Future Research

The research in this thesis is focus on a point-to-point communication system. It can be the next topic to study how to use compressed sensing to address the issue of a multiple access scenario. Moreover, it is assumed that the delay spread is limited within one frame duration so no intersymbol interference (ISI) occurs. Hence, the problem involving ISI can also be investigate in the future.

BIBLIOGRAPHY

BIBLIOGRAPHY

[1] R. Baraniuk, M. Davenport, R. DeVore, and M. Wakin. A simple proof of the restricted isometry property for random matrices. *Constr Approx*, 28(3):253–263, Dec 2008.

[2] R. Blazquez, F. S. Lee, D. D. Wentzloff, P. P. Newaskar, J. D. Powell, and A. P. Chandrakasan. Digital architecture for an ultra-wideband radio receiver. In *Vehicular Technology Conference, 2003. VTC 2003-Fall. 2003 IEEE 58th*, volume 2, pages 1303–1307, Oct 2003.

[3] E. J. Candes and J. Romberg. Sparsity and incoherence in compressive sampling. *Inverse Problems*, 23(3):969–985, Jun 2007.

[4] E. J. Candes, J. K. Romberg, and T. Tao. Stable signal recovery from incomplete and inaccurate measurements. *Comm. Pure Appl. Math.*, 59(8):1207–1223, Aug 2006.

[5] E. J. Candes and T. Tao. Decoding by linear programming. *IEEE Trans. Inform. Theory*, 51(12):4203–4215, Dec 2005.

[6] E. J. Candes and M. B. Wakin. An introduction to compressive sampling. *IEEE Signal Processing Mag.*, 25(2):21–30, Mar 2008.

[7] C. Carbonelli and U. Mengali. Synchronization algorithms for uwb signals. *Communications, IEEE Transactions on*, 54(2):329–338, Feb 2006.

[8] C. Carbonelli, U. Mengali, and U. Mitra. Synchronization and channel estimation for uwb signal. In *Global Telecommunications Conference, 2003. GLOBECOM '03. IEEE*, volume 2, pages 764–768 Vol.2, Dec 2003.

[9] S. S. Chen, D. L. Donoho, and M. A. Sauders. Atomic decomposition by basis pursuits. *SIAM J. Sci. Comput.*, 20(1):33–61, 1998.

[10] Mark A Davenport, Michael B Wakin, and Richard G Baraniuk. Detection and estimation with compressive measurements. *Dept. of ECE, Rice University, Tech. Rep*, 2006.

[11] D. Donoho. Compressed sensing. *IEEE Trans. Inform. Theory*, 52:1289–1306, Apr 2006.

[12] D. L. Donoho and X. Huo. Uncertainty principles and ideal atomic decomposition. *IEEE Trans. Inform. Theory*, 47(7):2845–2862, Nov 2001.

[13] M.F. Duarte, M.A. Davenport, M.B. Wakin, and R.G. Baraniuk. Sparse signal detection from incoherent projections. In *Acoustics, Speech and Signal Processing, 2006. ICASSP 2006 Proceedings. 2006 IEEE International Conference on*, volume 3, pages III–III, May 2006.

[14] W. Hirt and J.L. Massey. Capacity of the discrete-time gaussian channel with intersymbol interference. *Information Theory, IEEE Transactions on*, 34(3):38–38, 1988.

[15] R. Hoctor and H. Tomlinson. Delay-hopped transmitted-reference rf communications. In *Ultra Wideband Systems and Technologies, 2002. Digest of Papers. 2002 IEEE Conference on*, pages 265 – 269, 2002.

[16] J. A. Högbom. Aperture Synthesis with a Non-Regular Distribution of Interferometer Baselines. *aaps*, 15:417, June 1974.

[17] Ye (Geoffrey) Li, Andreas F. Molisch, Andreas F. Molisch, Jinyun Zhang, Jinyun Zhang, Senior Member, and Senior Member. Channel estimation and signal detection for uwb. In *Proc. IEEE WPMC*, 2003.

[18] Bing Liu, Ping Fu, Shengwei Meng, and Lunping Guo. Compressive sensing signal detection algorithm based on location information of sparse coefficients. *JDCTA*, 4(8):79–85, 2010.

[19] V. Lottici, A. D'Andrea, and U. Mengali. Channel estimation for ultra-wideband communications. *IEEE Journal of Selected Area in Communications*, 20(12):1638–1645, Dec. 2002.

[20] L.Yang and G. B. Giannakis. Ultra-wideband communications: An idea whose time has come. *IEEE Signal Process. Mag.*, 21:26–54, 2004.

[21] S. Mallat and Z. Zhang. Matching pursuits with time-frequency dictionaries. *IEEE Trans. Signal Process.*, 41:3397–3415, Dec 1993.

[22] Robert Matthews and Fiona Stones. Coincidences: the truth is out there. *Teaching Statistics*, 20(1):17–19, 1998.

[23] S. Mendelson, A. Pajor, and N. Tomczak-Jaegermann. Uniform uncertainty principle for bernoulli and sub-gaussian ensembles. *Constructive Approximation*, 28(3):277–289, Dec 2008.

[24] Andreas F. Molisch, Kannan Balakrishnan, Chia chin Chong, Shahriar Emami, Andrew Fort, Johan Karedal, Juergen Kunisch, Hans Schantz, Ulrich Schuster, and Kai Siwiak. IEEE 802.15.4a channel model – final report. In *Converging: Technology, work and learning. Australian Government Printing Service*, 2004.

[25] D. Needell and J.A. Tropp. Cosamp: Iterative signal recovery from incomplete and inaccurate samples. *Applied and Computational Harmonic Analysis*, 26(3):301 – 321, 2009.

[26] Ian O'Donnell, Mike S. W. Chen, Stanley B. T. Wang, and Robert W. Brodersen. An integrated, low power, ultra-wideband transceiver architecture for low-rate, indoor wireless systems. In *IEEE CAS Workshop on Wireless Communications and Networking*, September 2002.

[27] J. L. Paredes, G. R. Arce, and Z. Wang. Ultra-wideband compressed sensing: Channel estimation. *IEEE Journal of Selected topics in Signal Processing*, 1(3):383–395, 2007.

[28] A. Rabbachin and I. Oppermann. Synchronization analysis for uwb systems with a low-complexity energy collection receiver. In *Ultra Wideband Systems, 2004. Joint with Conference on Ultrawideband Systems and Technologies. Joint UWBST IWUWBS. 2004 International Workshop on*, pages 288–292, May 2004.

[29] J.A. Tropp and A.C. Gilbert. Signal recovery from random measurements via orthogonal matching pursuit. *Information Theory, IEEE Transactions on*, 53(12):4655–4666, Dec 2007.

[30] A.M. Tulino, G. Caire, S. Shamai, and S. Verdu. Capacity of channels with frequency-selective and time-selective fading. *Information Theory, IEEE Transactions on*, 56(3):1187–1215, 2010.

[31] Lin Wu, Xianren Wu, and Zhi Tian. Asymptotically optimal UWB receivers with noisy templates: design and comparison with rake. *Selected Areas in Communications, IEEE Journal on*, 24(4):808 – 814, april 2006.